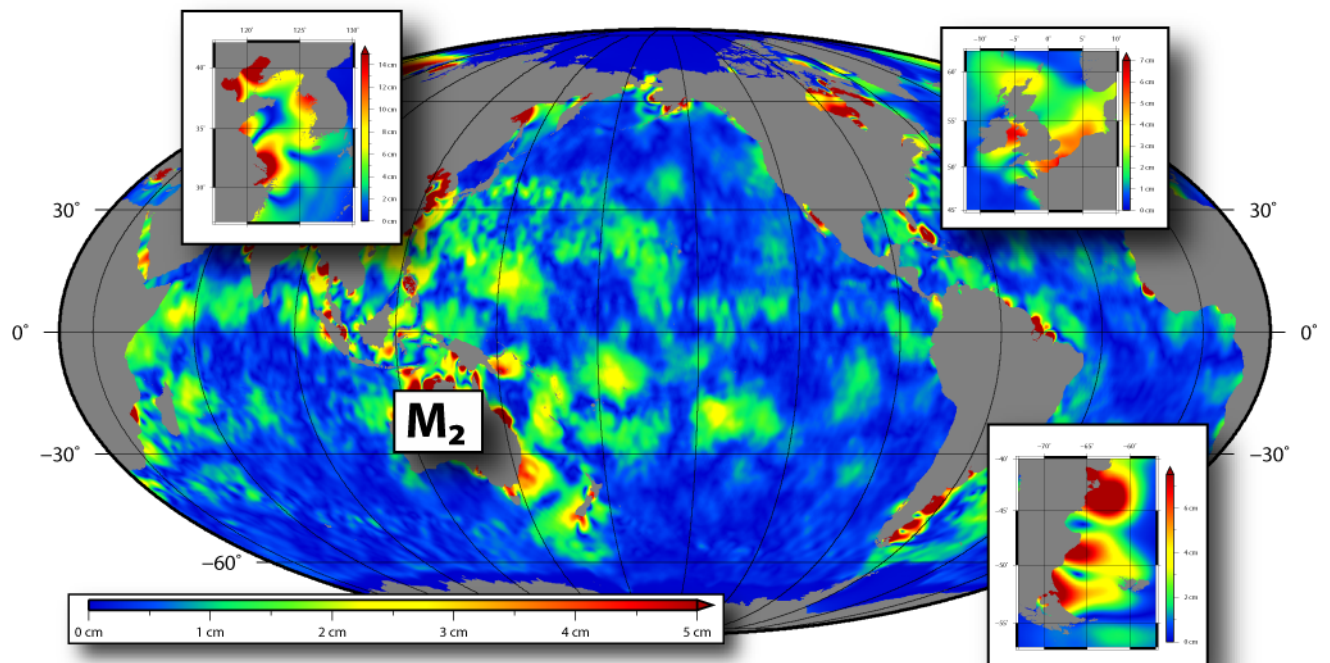


DGFI REPORT
No. 89

EOT11A - EMPIRICAL OCEAN TIDE MODEL FROM MULTI-MISSION
SATELLITE ALTIMETRY

ROMAN SAVCENKO AND WOLFGANG BOSCH



Residual amplitudes of M_2 tidal constiuent of EOT11a wrt. FES2004



DEUTSCHES GEODÄTISCHES FORSCHUNGSINSTITUT (DGFI)
ALFONS-GOPPEL-STR. 11, D-80539 MÜNCHEN, GERMANY

2012

Abstract

EOT11a is a new global solution for the amplitudes and phases of the most dominant ocean tide constituents based on an empirical analysis of multi-mission satellite altimetry data. EOT11a benefits from FES2004, a hydrodynamic model widely used for altimetry and long time taken as reference model in GRACE gravity field modeling. In shallow water areas the M_2 and S_2 constituents show numerous extended patterns with residual amplitudes of up to 15 cm. Other major constituents and the non-linear shallow water tide M_4 hit residual amplitudes up to 5 cm. Validation at altimeter crossovers and with independent bottom pressure data confirm the significance of these findings. A correlation analysis proves the separability of the analyzed constituents.

Contents

1	Introduction	4
2	Residual tide analysis of altimeter data	5
2.1	Altimeter data pre-processing	6
2.2	Harmonic Analysis	7
2.2.1	Functional model	7
2.2.2	Least squares approach	7
2.2.3	Stochastic model	8
2.2.4	Decimation of measurements	8
2.2.5	Variance component estimate	9
2.2.6	Data editing and outlier elimination	9
2.3	Results	10
2.4	Comparison with the tidal constants	11
2.5	Correlation analysis	12
2.6	Computation of loading and ocean tides	14
3	Composition of EOT11a	15
4	Differences between EOT08a and EOT11a	16
5	Validation and comparison with other tide models	17
6	Conclusions	22
7	Acknowledgement	27
A	Appendix	27
A.1	Patagonian shelf	28
A.2	North-West European Shelf	30
A.3	Yellow Sea	32
A.4	Long period tides in shallow water areas	34
A.5	Global Maps	35
A.6	Mission specific mean values	48

1 Introduction

The knowledge of ocean tides is of fundamental importance as the gravitational attraction of Sun and Moon causes more than 80% of the total variability of the sea surface (Le Provost 2001). Prediction of ocean tides is crucial for the coastal environment and the protection of its ecosystem, the livelihood of many millions of people. But knowledge of ocean tides is also needed for the precise treatment of space observations. Global ocean tide models quantify loading effects for stations on land, and explain part of the variation observed in Earth rotation. Altimetric sea surface heights are to be de-tided in order to be comparable with each other, to allow assimilation into numerical models, and to estimate the mean sea surface. Also, the precise modeling of the Earth gravity field requires reducing not only the direct potential of Sun and Moon, but also the gravitational potential caused by the tidal re-distribution of water masses. The latter is of particular concern in the analysis of data of the GRACE mission. As the ocean tides (with periods of about 12 and 24 hours) are only rarely sampled by GRACE, the tidal signal (and their errors) can be recognized only after rather long “alias” periods. The uncertainties in the tide model are supposed as a possible reason for the meridional stripes which are still present in all satellite-only gravity field solutions obtained from GRACE data. To improve this situation is the basic motivation of the investigations presented here. This report compiles results obtained in the context of COTAGA, a project of the priority program “Mass transport and mass distribution in the Earth system”, funded by the Deutsche Forschungsgemeinschaft (DFG).

Substantial progress in modeling of ocean tides has been achieved through the analysis of increasingly long time series of satellite altimetry data and refinements in hydrodynamic modeling. This progress is indicated by a considerable number of improved ocean tide models, e.g. GOT99.2b and GOT00.2 (Ray 1999), NAO99 (Matsumoto u. a. 2000), CSR4.0 (Eanes 1994), FES2002 (Le Provost 2002), FES2004 (F. Lyard u. a. 2006), TPXO6.2 (Egbert und Erofeeva 2002). TPXO7.2 (Egbert 2010) and GOT4.7 (Ray 1998) are the latest revisions of the TPXO and GOT model series. In general ocean tides are known in deep ocean to within 2cm rms at wavelengths of 50 km (Shum u. a. 1997). However, in coastal regions, over continental shelves and in polar oceans tides are significant less known. Current investigations show that all state-of-the-art ocean tide models

- have significant errors for S_2 and M_2 e.g. in Antarctica (Wünsch u. a. 2005; King und Padman 2005) which are due to poor or missing altimetry and tide data at high latitudes,
- have alias frequencies (with GRACE) much longer than 30 days for S_2 and K_2 leaving the errors of these constituents almost unreduced in monthly gravity field solutions (Knudsen 2002), (Mayer-Gürr, 2005, unpublished), and
- are still not able to predict the water level in shallow water with sufficient precision (Savcenko und W.Bosch 2004).

There are clear indications, however, that these problems can be remedied: (Han u. a. 2005) already demonstrated that it is possible to solve for S_2 and M_2 tides with a spatial resolution as short as 300 km from GRACE data only. Andersen (1999) and Smith (2000) have shown that it is possible to improve the ocean tide models in shallow water and to estimate also nonlinear terms like M_4 . The TOPEX altimeter mission observed for more than 10 years over the same ground track allowing to resolve and separate all dominant tidal constituents. In February

2002 Jason-1 continued observations over the same ground track while a few months later the TOPEX orbit was shifted in order to double the spatial resolution. Jason-2 was launched and is observing over the original TOPEX ground track, while Jason-1 has been moved to an interleaved ground track. Tide analysis with altimeter data from original and interleaved ground track systems are now capable to provide significant improvements for the dominant tidal constituents and non-linear shallow water effect like M_4 and M_6 .

The GRACE Science Data System processing centres at CSR, GFZ, and JPL agreed to use FES2004 for de-aliasing of the release 04 GRACE gravity field solutions. At that time FES2004 has been shown to perform better than other recent models like CSR4.0 or GOT00. The model has been also used for altimetry data. In fact to harmonize the multi-mission data base maintained at DGFI the ocean tide corrections of all altimeter systems have been computed with the FES2004 model (the improved release with K_2 taken from FES2002 and S_1 replaced). This is the reason why in this study FES2004 is still taken as a reference and a tidal analysis is performed for the residuals only.

2 Residual tide analysis of altimeter data

Two methods can be used for the empirical estimates of tides, least squares harmonic analysis and the so called response method - each one with its own pros and cons. While the response method (Cartwright 1990; Desai und Wahr 1995; Smith 1999) aims to determine the whole diurnal and semidiurnal spectra, the harmonic analysis estimates amplitudes and phases of particular tidal constituents with predefined periods (Schrama und Ray 1994; Ray 1999). The response method is more appropriate for estimating weak tides. However, it is not applicable for a global estimation of nonlinear tides: the assumption of a smooth admittance function is violated in some parts of the ocean – the admittances can even exhibit strong resonant peaks and some nonlinear tidal constituents coincide with astronomical tides. Compared to precise tide gauge records the signal to noise ratio of altimeter data is still too low for identifying minor tidal constituents. Neglecting minor tides leads – in general – to background noise, however in case of a residual tide analysis this background noise is significantly mitigated: The a priori tide model takes care of minor tides using the admittance theory. Because this study focuses on improvements over shallow water where the assumption of a smooth admittance is difficult to justify the harmonic analysis is applied here (see section 3.2)

The tide analysis with altimeter data faces two general difficulties - the alias effect and the problem of de-correlating tidal signals with alias periods very close to each other. Alias effects emerge if the altimeter systems sample high frequency tide signals with periods of some 12 and 24 hours only every few days (the satellite repeat period). In this case the tides appear as signals with periods much longer than the sampling interval. These periods – called alias periods – are different for the tidal constituents and depend on the repeat period of the altimeter satellite, see tabulated alias periods in Smith (1999) and Andersen (1999). The capability to separate neighbouring periods from each other is expressed by the Rayleigh criterion. In case of the empirical tide analysis by altimetry the Rayleigh criterion must be applied to the alias periods. The minimal time span needed for the accurate separation of two tides is called Rayleigh period. For the tidal analysis of altimeter data these periods can again become very large – even infinite if one of the tidal signals cannot be de-aliased at all. A comprehensive discussion on the alias and Rayleigh periods can be found in Smith (1999). With some thirteen years the altimeter time series on the TOPEX ground tracks (observed by TOPEX and its follow-on, Jason1) is

long enough to dealias all major tidal constituents and also fulfils the Rayleigh criterion for their de-correlation. The time series of 35-day repeat periods of the sun synchronous missions ERS and ENVISAT are, however, problematic in resolving and separating several tidal constituents. The tide constituents S_2 , K_1 and P_1 are affected by severe correlation problems and cannot be estimated using the data of these missions alone. The M_2 and N_2 tides can be separated from each other only if at least a nine years time series of data is available. The difficulties on alias and Rayleigh periods apply if the data of a single mission at a particular point is considered. Using data on crossing or adjacent tracks already improves the temporal resolution and can in general mitigate the alias effect. The advantage of a complementary sampling on single satellite crossover points depends of the tidal constituent and the latitude (Smith 1999). The most efficient solution to de-alias and de-correlate the constituents is achieved by combining time series of missions with different sampling characteristics. This combination requires a careful preprocessing of altimeter data which is briefly described in the following section.

2.1 Altimeter data pre-processing

The tidal analysis was based on the common use of altimeter data of TOPEX, Jason-1, Jason-2, ERS-2, ENVISAT (see tab.1). Combining altimeter data of different missions requires at least two pre-processing steps: upgrading and harmonization.

Upgrading means to use the most recent (re-tracked) observation data, mission specific correction models, and orbital ephemerides. For the ESA missions new orbits were taken from (Scharroo und Visser 1998). All ERS-1 and ERS-2 specific corrections recommended by (Schrama u. a. 2000) have been applied. The wet tropospheric correction for ERS-2 were computed using the algorithm described in (Eymard u. a. 2003). The orbits of ENVISAT were replaced by GRACE-based orbits from DEOS. Since these orbits are available only up to 64-th cycle the data of other cycles weren't taken into account. Because of the significant change in the processing software the ENVISAT mission was considered as two missions ENVISAT/GDR-A (cycles 009-037) and ENVISAT/GDR-B (cycles 038-064). For TOPEX, the sea state bias model described by (Chambers u. a. 2003) was used and the wet tropospheric correction were taken from the JPL "microwave replacement product", version 1.0 (Desai, pers. communication).

Harmonization implies to use as far as possible the same models for geophysical corrections to avoid that model differences are interpreted as apparent sea level variations. Therefore, for all missions the inverted barometer correction was replaced by the dynamic atmospheric corrections (DAC) produced by CLS Space Oceanography Division using the MOG2D model from LEGOS (L. Carrère und Lyard 2003). As already indicated, the ocean tide corrections for all missions were based on the FES2004 (F. Lyard u. a. 2006). All time series analysis are performed with sea level anomalies, deviation of the instantaneous sea level from a mean sea

Mission	Cycles	Period	Source
TOPEX/Poseidon	001 - 481	1992/09/23 - 2005/10/08	MGDR-B (NASA)
Jason-1	001 - 291	2002/01/15 - 2009/12/04	GDR-C (NASA,CNES)
Jason-2	000 - 064	2008/07/04 - 2010/04/07	GDR (CNES)
ERS-2	000 - 085	1995/04/29 - 2003/07/02	OPR-V6 CERSAT
ENVISAT	009 - 064	2002/09/24 - 2008/01/07	GDR-A,GDR-B ESA/CNES

Table 1: Altimeter data used in this study

surface. For all altimeter mission the CLS01 mean sea surface (Hernandez und Schaeffer 2000) was taken as a reference for sea level anomalies.

2.2 Harmonic Analysis

The residual least-squares harmonic analysis has been applied. The radial error component was not corrected because the available sets of radial corrections based on MMXO10 exhibit significant tidal signals identified by means of along-track analysis of TOPEX/Poseidon data. Instead, mission specific mean values were introduced by means of computation of the different mean values for each grid node. The abdication of cross-calibration mitigates the de-correlation capacity of this type of analysis. A comparative judgment between local mission specific biases and global range biases of cross-calibration remains a subject for future investigations.

2.2.1 Functional model

The harmonic analysis was applied for the constituents M_2 , S_2 , N_2 , K_2 , $2N_2$, K_1 , O_1 , Q_1 , P_1 , S_1 , M_f , M_m and M_4 . In addition to the sine and cosine coefficient of these constituents, six mean values (TOPEX/Poseidon, Jason-1, Jason-2, ERS-2, ENVISAT/GDR-A and GDR-B), and annual and semi-annual signals were solved simultaneously.

The functional model can be described by means of the following observation equation:

$$\begin{aligned} \zeta(t, \phi, \lambda) + v &= m_{mis}(\phi, \lambda) \\ &+ \sum_{i=1}^n (h_{1i} f_i(t)(\phi, \lambda) \cos(\omega t_i + u_i(t)) + h_{2i} f_i(t)(\phi, \lambda) \sin(\omega t_i + u_i(t))) \\ &+ \sum_{j=1}^2 (H_{1j}(\phi, \lambda) \cos(\Omega t_j) + H_{2j}(\phi, \lambda) \sin(\Omega t_j)), \end{aligned} \quad (1)$$

where

$\zeta(t, \phi, \lambda)$	estimated sea level anomaly (de-tided by FES2004)
v	estimated residual
$m_{mis}(\phi, \lambda)$	mission specific mean value
t	time
ωt_i	astronomical arguments
h_{1i}, h_{2i}	cosine and sine coefficients of tidal constituents
$f_i(t), u_i(t)$	nodal corrections to amplitude and phase
Ω_j	angular frequency for annual and semiannual variations
H_{1j}, H_{2j}	cosine and sine coefficients of annual and semiannual variations

2.2.2 Least squares approach

The least-squares approach applied to Eq. 2.2.1 can be described by means of

$$\mathbf{N}\mathbf{x} = \mathbf{y}. \quad (2)$$

with the normal equation

$$\mathbf{N} = \mathbf{A}'\mathbf{P}_{bb}\mathbf{A} \quad (3)$$

and the right-hand vector

$$\mathbf{y} = \mathbf{A}'\mathbf{P}_{\mathbf{bb}}\mathbf{w}, \quad (4)$$

with

- \mathbf{x} vector of unknowns
- \mathbf{A} design matrix describing of linearized observation equations
- \mathbf{w} observation vector containing of measured sea level anomalies
- $\mathbf{P}_{\mathbf{bb}}$ dispersions matrix of measurements

2.2.3 Stochastic model

To mitigate the correlation problem the analysis was performed on the nodes of a regular $15' \times 15'$ geographical grid. For every grid node normal equations were accumulated using all observations inside a spherical cap and applying a Gauss function for weighting inverse proportional to the spherical grid node distance ψ :

$$w_{dist} = e^{-\sigma\psi^2} \quad (5)$$

with

$$\sigma = \ln(2)\tau^{-2}. \quad (6)$$

τ is the half weight width controlling the decay of the Gauss function. ψ is the spherical distance to the node.

The selection of the limiting cap radius ψ_{max} and the decay τ is critical: high weights and a large cap size imply a strong smoothing. Low weights and a small cap size can prevent the desired de-correlation of some constituents. Additionally low signal-to-noise-ratio for weak tidal constituents makes it necessary to introduce a strong spatial smoothing. To achieve optimal results of tidal estimation different weighting parameters were considered. For the EOT11a half weight width of τ was set to 0.5° , 1° and 1.5° were tested. Because of the shape of the weighting function (eqn. 5) the ratio between the limiting cap radius and half weight width

$$\tau = 0.3 \cdot \psi_{max} \quad (7)$$

was chosen for all computations.

2.2.4 Decimation of measurements

The results of multi-mission-crossover analysis demonstrate that the altimeter measurements exhibit a high correlation along track. This is due to instrumental and environment corrections which are certainly not free for errors. The correlation functions exhibit a very complicated character and are depending on the geographical position and the time. Therefore no a priori correlation information were used. Neglecting correlations leads automatically to the unrealistic error propagation. Therefore the correlations were considered by a weighted mean of all measurements of one pass lying inside the spherical cap. The formula 5 was used for the computation of the weights. The effect of large slopes of sea surface was mitigated because the analysis was applied on the sea surface anomalies. The small time difference between subsequent measurements can be neglected in the context of tide analysis. Therefore the time of the measurement closest to the grid node was taken as observation time of the mean value.

2.2.5 Variance component estimate

A proper weighting of the data of different missions i , $i = 1, \dots, k$, was achieved by the variance component estimate. The formulae are given in (Eicker 2008). The accumulated normal equations are composed of weighted normal equations of individual missions,

$$\mathbf{N} = \sum_{i=1}^k \frac{1}{\sigma_i^2} \mathbf{N}_i \quad \mathbf{y} = \sum_{i=1}^k \frac{1}{\sigma_i^2} \mathbf{y}_i. \quad (8)$$

The variance components can be obtained iteratively by

$$\hat{\sigma}_i^2 = \frac{\Omega_i}{r_i}. \quad (9)$$

Where r_i is the partial redundancy and

$$\Omega_i = \hat{\mathbf{v}}' \mathbf{P}_{\mathbf{bb}} \hat{\mathbf{v}}. \quad (10)$$

Where $\hat{\mathbf{v}}$ is the vector of residuals and $\mathbf{P}_{\mathbf{bb}}$ is the dispersions matrix of measurements. To compute the partial redundancy the following formula can be used.

$$r_i = n_i - \frac{1}{\sigma_i^2} \text{tr}(\mathbf{N}_i \mathbf{N}^{-1}) \quad (11)$$

Where n_i is the number of the measurements of one mission. The variance component estimate can be realized by iteration because both the unknowns $\hat{\mathbf{x}}$ and the variances of normal equations $\hat{\sigma}_i^2$ are initially unknown.

2.2.6 Data editing and outlier elimination

To edit the altimeter data the following criteria were used. The standard deviation of altimeter range should be less than 0.3 m. The absolute value of sea level anomalies was limited to ± 2.5 m. The land data were excluded by means of sensor flags and a land ocean mask obtained from GMT (Wessel und Smith 1996). The critical aspect of data editing is the flag signaling the measurements over the ice. Unfortunately these flags were not suitable for all missions leading to the use of corrupt measurements. To avoid this problem two sequential outlier test were carried out. The first test is a very coarse checking of the ice contamination. For this purposes the mean and standard deviation were computed for the missions with good ice flags. All data of all missions with the differences from estimated mean larger than the quadruple standard deviation were considered as ice contaminated. The main problem for this kind of tests is the relative biases. They make the standard deviations too large. To avoid the influence of relative biases an arbitrary set of mean relative biases were applied. Although they don't correct the radial error components they make the confidence intervals for measurements sufficiently realistic. The second outlier test was applied using the functional model of tidal analysis. The measurements with the residuals larger than three times the standard deviation were considered as outlier.

2.3 Results

Some preliminary investigations performed in the North-West European and the Patagonian Shelves indicated that in shallow water the residual amplitudes w.r.t to FES2004 can exceed the decimeter level. This was confirmed by the global analysis of multi-mission altimeter data. Significant residuals were found for all estimated tidal constituents. Even for such weak tide as $2N_2$ residuals of 1-2 cm were identified.

As mentioned in the section 2.2.3 the choice of the weighting parameters (the cap size as well as the half weight width) is a critical aspect for the tidal analysis. An analytical derivation of these parameters is impossible. We therefore apply an empirical variation accounting for the spatial distribution of altimeter data. First of all, the distribution of multi-mission-altimeter data is different in different parts of ocean and depends not only on latitude.

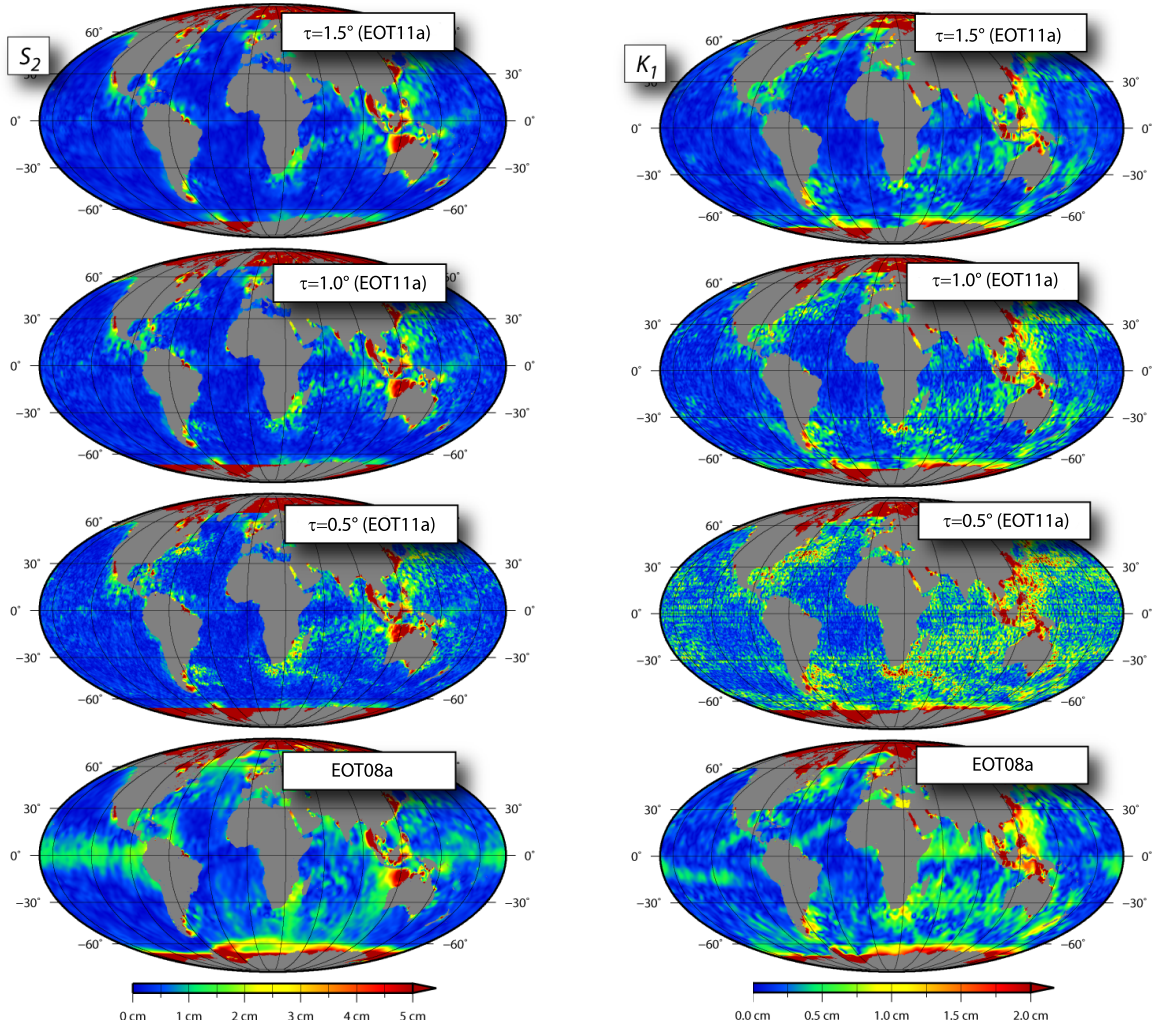


Figure 1: Residual S_2 from solutions with different τ of EOT11a and EOT08a

Figure 2: Residual K_1 from solutions with different τ of EOT11a and EOT08a

Also each mission has its own strengths and weaknesses in different parts of ocean (e.g. wet tropospheric correction is critical in the coastal areas). Finally, each mission covers different time periods, a critical aspect for the de-correlating of those tidal constituents strongly cor-

related with meteorological signals like annual and semi-annual variation of sea surface. The tests of weighting parameters show that in some cases it is necessary to use large cap size and half weight width to achieve better de-correlations on the cost of a degradation of spatial resolution.

The three upper panels of figure 1 show the effect of the weighting parameters on the estimation of S_2 tidal constituent. The half weight width of 0.5° is too small because of sun-synchronous ESA orbits. Therefore some artificial effects can be seen in this solution. In other case the half weight width of 1.5° is too large leading to a very smooth solution. All three solutions don't exhibit the artificial effects in the equatorial areas and in the polar regions at the seasonal ice boundaries. The tidal constituent K_1 shown in figure 2 is strongly correlated with season effects in time series of all mission. Therefore the results with small weights are useless. The results of the estimation using of half weight width of 1.0° of 1.5° don't show pattern presented in the results of harmonic analysis of EOT08a. It is impossible to evaluate which of the both solution is better looking at the geographical pattern only. Therefore it is important to validate the results by means of external data.

2.4 Comparison with the tidal constants

For the validation of each solution three sets of tidal constants were available. The first set is ST102 (Ray, private communication, 2007) suitable for validation of global tide model over the deep ocean. The next data set is the pelagic tidal constants from IAPSO (Smithson 1992). The distribution of these constants is less homogeneous but these tide gauges allows better validation over shallow water areas. The last set of tidal constants are the coastal tidal constants from WOCE (Ponchant und Lyard 2008). These data contain the local information in coastal areas. Nevertheless the comparisons can provide the mean statistic information. The geographical distribution of tidal constants can be seen in figure 3. Caused by the length of time series used for tide analysis not all tidal constants are present at shown positions.

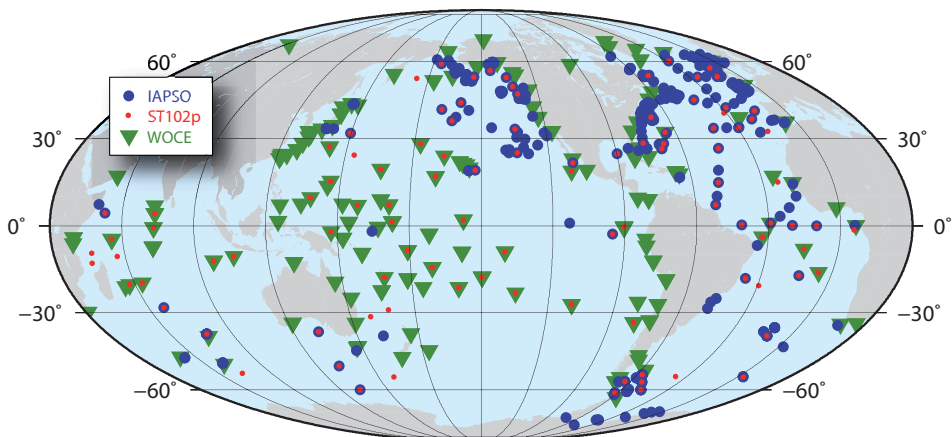


Figure 3: Positions of available tidal constants

All available tidal constants are ocean and not geocentric tidal. Therefore the ocean tide grids were computed for all results. All loading and ocean tides were added to results to get elastic ocean tides. The ocean tides were computed by means of subtraction of computed loading tides from elastic ocean tides (see section 2.6). As positions of independent data don't agree with

the grid nodes the results were interpolated for position of tide gauges. The linear interpolation was chosen. The complex tidal constants at the point $P(\phi, \lambda)$ is

$$tc(\phi, \lambda) = \frac{\sum_{i=1}^2 \sum_{j=1}^2 w_{ij} \cdot tc_{ij}}{\sum_{i=1}^2 \sum_{j=1}^2 w_{ij}}. \quad (12)$$

Where tc_{ij} are complex tidal constants at the neighboring grid nodes. w_{ij} are the linear weights computed by means of

$$w_{ij} = \left(1 - \frac{d_\phi}{\Delta\phi}\right) \cdot \left(1 - \frac{d_\lambda}{\Delta\lambda}\right). \quad (13)$$

$\Delta\phi$ and $\Delta\lambda$ are the grid steps. Where d_ϕ and d_λ are coordinate differences of grid nodes and tide gauge positions. To compare amplitudes A_i^s and phases Φ_i^s for individual constituents i of solutions with $\tau = 0.5^\circ, 1^\circ, 1.5^\circ$ the RMS differences to the tidal constants were computed by means of the following formula

$$RMS = \sqrt{\frac{\sum_{i=1}^n \left(\left(A_i^{tg} \cos \Phi_i^{tg} - A_i^s \sin \Phi_i^s \right)^2 + \left(A_i^{tg} \sin \Phi_i^{tg} - A_i^s \cos \Phi_i^s \right)^2 \right)}{2n}} \quad (14)$$

where A_i^{tg} and Φ_i^{tg} are the tidal constants from tide gauges. A_i^s and Φ_i^s stand for the tidal constants of each individual solutions.

Tide	ST102p			IAPSO			WOCE		
	0.5°	1.0°	1.5°	0.5°	1.0°	1.5°	0.5°	1.0°	1.5°
M_2	1.448	1.426	1.430	2.490	2.507	2.531	11.955	11.852	11.754
S_2	1.467	0.846	0.832	2.302	2.018	2.014	7.965	4.181	4.180
N_2	0.659	0.641	0.639	1.030	1.014	1.012	2.598	2.569	2.527
K_2	0.458	0.423	0.412	0.931	0.886	0.884	1.450	1.482	1.515
$2N_2$							0.562	0.531	0.526
K_1	0.969	0.957	0.961	1.831	1.817	1.820	3.919	3.948	4.019
O_1	0.734	0.729	0.720	1.453	1.472	1.483	2.908	2.967	3.004
P_1	0.452	0.377	0.369	2.594	2.594	2.601	1.299	1.298	1.310
Q_1	0.354	0.295	0.276	0.526	0.494	0.488	0.693	0.681	0.681
S_1							3.120	0.499	0.443
M_4							1.274	1.402	1.462
M_m							0.907	0.882	0.866
M_f							0.777	0.744	0.735

Table 2: RMS differences between tidal constants of solutions for $\tau = 0.5^\circ, 1^\circ, 1.5^\circ$ and independent data

2.5 Correlation analysis

As multi-mission altimetry is used for this study there is a complete irregular distribution of observations along the ground tracks contributing to each grid node. Consequently there is no simple rule to examine the potential to identify and separate all tidal constituents. It is

	m_{tp}	m_{j_1}	m_{j_2}	m_{ers2}	m_{ena}	m_{enb}	M_2	S_2	N_2	K_2	$2N_2$	O_1	K_1	P_1	Q_1	S_1	M_f	M_m	M_4	S_a	S_{sa}
m_{tp}		0.01	0.01	0.01	0.01	0.00	0.01	0.01	0.01	0.01	0.01	0.01	0.01	0.01	0.01	0.02	0.01	0.01	0.01	0.02	0.01
m_{j_1}			0.01	0.01	0.01	0.01	0.01	0.02	0.01	0.03	0.01	0.01	0.04	0.03	0.01	0.03	0.01	0.01	0.01	0.06	0.05
m_{j_2}				0.01	0.01	0.01	0.01	0.01	0.00	0.02	0.00	0.00	0.02	0.01	0.01	0.01	0.00	0.00	0.00	0.05	0.04
m_{ers2}					0.31	0.31	0.02	0.44	0.01	0.02	0.01	0.01	0.01	0.01	0.01	0.06	0.01	0.01	0.01	0.02	0.02
m_{ena}						0.26	0.02	0.35	0.01	0.02	0.01	0.01	0.01	0.01	0.01	0.05	0.01	0.01	0.01	0.04	0.02
m_{enb}							0.02	0.35	0.01	0.01	0.01	0.01	0.01	0.01	0.02	0.05	0.01	0.01	0.01	0.05	0.01
M_2							0.04	0.03	0.01	0.01	0.01	0.01	0.01	0.01	0.02	0.01	0.02	0.01	0.01	0.01	0.01
S_2								0.02	0.02	0.01	0.01	0.01	0.01	0.01	0.02	0.08	0.01	0.01	0.01	0.01	0.01
N_2									0.01	0.01	0.01	0.02	0.01	0.01	0.01	0.01	0.01	0.01	0.01	0.01	0.01
K_2										0.01	0.01	0.01	0.05	0.08	0.01	0.02	0.01	0.01	0.01	0.02	0.29
$2N_2$											0.01	0.01	0.02	0.01	0.01	0.01	0.01	0.01	0.01	0.02	0.01
O_1												0.01	0.01	0.01	0.01	0.01	0.02	0.01	0.01	0.01	0.01
K_1													0.01	0.29	0.01	0.03	0.01	0.01	0.01	0.06	0.07
P_1															0.02	0.03	0.01	0.01	0.01	0.06	0.05
Q_1																0.01	0.01	0.02	0.02	0.01	0.01
S_1																	0.01	0.01	0.01	0.01	0.01
M_f																	0.01	0.01	0.01	0.01	0.01
M_m																		0.01	0.03	0.01	0.01
M_4																					
S_a																				0.01	0.01
S_{sa}																				0.01	0.03

Table 3: Mean correlations for the half weight width of 0.5°

therefore essential to analysis the correlations among the constituents. According to Smith (1999) the correlation between two constituents are defined as RMS of the correlation between their sine and cosine coefficients.

$$\rho = \sqrt{\frac{1}{4} (\rho_{c_1, c_2}^2 + \rho_{s_1, s_2}^2 + \rho_{c_1, s_2}^2 + \rho_{s_1, c_2}^2)} \quad (15)$$

Similar, the correlation between tides and mean sea level is defined by following formula

$$\rho = \sqrt{\frac{1}{2} (\rho_{c, m}^2 + \rho_{s, m}^2)} \quad (16)$$

The global mean values of these correlation have been compiled to the table 3. For most of the constituents the mean correlation remains well below 0.05. Correlations above 0.2 appear only between S_2 and the mean value, K_2 and the semi-annual variation, S_{sa} , and between K_1 and P_1 . The latter is caused by the sun-synchronous orbits of ERS and ENVISAT, causing alias periods of about one year for both tides. This implies an infinite Rayleigh period – a separation is only possible by means of satellites with different orbit configuration.

2.6 Computation of loading and ocean tides

The tides observed by altimeter are geocentric tides which are the sum of the solid earth tide, pole tide, ocean and loading tides. Because the solid earth tides are well modeled and pole tides don't coincide with ocean tide spectra, only loading and ocean tides were considered. The results of residual tide analysis are the residual elastic ocean tides. Therefore to obtain the loading or ocean tides one of both should be computed from elastic tides. We decide to use the algorithm described in Cartwright und Ray (1991). To achieve a better spatial resolution the spherical harmonic decomposition up to degree 720 was used for EOT11a. The complex elastic ocean tide admittance decomposed in complex spherical harmonics can be described by means of the following formula

$$Z(\phi, \lambda) = \sum_{n, m} a_{n, m} Y_{nm}(\phi, \lambda). \quad (17)$$

The spherical harmonic admittances of ocean tides can be described by means of

$$Z_o(\phi, \lambda) = \sum_{n, m} a_{n, m}^o Y_{nm}(\phi, \lambda). \quad (18)$$

The load tide admittance can be described by

$$Z_l(\phi, \lambda) = \sum_{n, m} \alpha_n a_{n, m}^o Y_{nm}(\phi, \lambda), \quad (19)$$

where $\alpha_n = \frac{3}{2n+1} \frac{\rho_w}{\rho_e} h'_n$. The love numbers h'_n were taken from Farrell (1972). The load tides can be computed by means of

$$Z_l(\phi, \lambda) = \sum_{n, m} \beta_n a_{n, m}^o Y_{nm}(\phi, \lambda), \quad (20)$$

where $\beta = \frac{\alpha_n}{1+\alpha_n}$. After synthesis of loading admittances the ocean admittances were computed as the difference of elastic and loading admittances:

$$Z_o(\phi, \lambda) = Z(\phi, \lambda) - Z_l(\phi, \lambda). \quad (21)$$

3 Composition of EOT11a

For the composition of EOT11a there were three solutions. Because of the low correlation (c.f. section 2.5) the tidal constituents of each solution can be individually selected for the final model. Accounting to the different half weight widths there were three different solutions for the final composition of EOT11a. Although the comparisons with tide gauges give some valuable information about quality of results they can be taken for the orientation only because each tide gauge is representative for a local area only.

Tide	τ	r_{max}	mask type
M_2	1.0°	3.0°	a
S_2	1.0°	3.0°	b
N_2	1.0°	3.0°	a
K_2	1.0°	3.0°	a
$2N_2$	1.5°	4.5°	a
O_1	0.5°	1.5°	a
K_1	1.0°	3.0°	b
P_1	1.5°	4.5°	b
Q_1	1.5°	4.5°	a
S_1	1.5°	4.5°	b
M_4	0.5°	1.5°	a
M_m	1.5°	4.5°	a
M_f	1.5°	4.5°	a

Table 4: Composition of EOT11a

Only the exceptional large or exceptional small RMS values can be essential criteria for accepting or declining of some grids. Therefore we decide to use the grid computed with half weight width $\tau = 1.0^\circ$ general for all semi-diurnal tides. The exception is $2N_2$ because this tide is very weak and coincides with some shallow water tides. The diurnal tides P_1 , Q_1 and S_1 were taken from the smoothest solution because of very low signal-to noise-ratio of available data. The smallest weighting parameters are appropriate for O_1 because this tide can be separated from main missions. The half weight width of 1.0° is more or less good compromise for K_1 . Because of short wave length the smallest weighting parameters should be used for M_4 . The long period tides exhibit small residual signals and long wavelengths therefore the largest tested influence radius is used. The table 4 summarizes the composition of EOT11a.

The sea surface is covered by permanent and seasonal sea ice. Because of the problems with the flags indicating ice measurements some time series were seriously affected by invalid measurements. This lead to unrealistic estimation of tides in such areas. In order to reject corrupt estimations two ice masks were used. The first mask *a* was obtained from NSIDC seasonal ice masks and is equal to the minimum extension ice mask extended by smooth transition zones with the width of 30 km in order to avoid discontinuity at the ice boundaries. Because of strong correlation problems of time series sun synchronous altimeter missions the tides S_1 , S_2 , K_1 , and K_1 couldn't be estimated precisely in polar regions. Therefore these tides were corrected by the second mask *b*, which is the minimum extension ice mask for the areas covered by TOPEX and Jason data. These two masks are shown in figure 4.

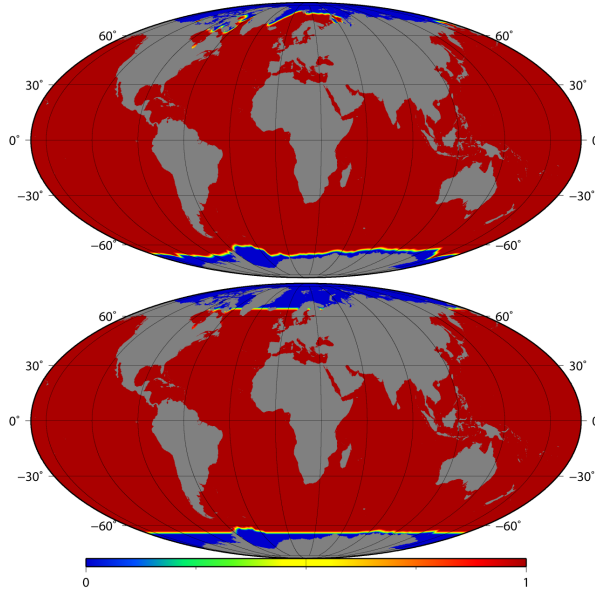


Figure 4: Masks used for EOT11a: a) general mask, b) mask for S_1 , S_2 , K_1 , and K_2

4 Differences between EOT08a and EOT11a

The both tide models EOT08a and EOT11a were obtained using harmonic analysis based on data from the DGFII OpenADB data base system. But there are more differences between these models than similarities.

First of all the EOT08a was obtained from cross-calibrated data. No cross-calibration was used for the both EOT10a and EOT11a models. To save computer capacity in case of EOT08a the normal equations were computed for each measurement and accumulated at the grid nodes without saving the original observations. This way is very efficient but there are no possibilities for some statistical outlier tests and the variance component estimate. Therefore the data used for EOT11a were reorganized in advance in order to allow an efficient access in an arbitrary area. The time series were created for each grid node. In the first step the outlier were eliminated to allow robust procedure and the mean mission specific offsets are added to each mission leading to smaller standard deviation and reducing the the confidence limits. Then the measurements were decimated as described in section 2.2.4. Then the normal equation matrices were accumulated for each averaged measurement. Because the time series of averaged measurements were still available the variance component estimate could be carried out.

The next differences between models consists in the tides S_1 , M_m , and M_f estimated for EOT10a and EOT11a only. The weighting of EOT08a depends on bathymetry. For EOT11a the unique weighting for different solutions was used. For EOT08a the data of different missions were considered as the common virtual system and therefore no mission specific parameters were estimated. The mission specific mean values were estimated for EOT11a in order to capture geographic correlated orbit errors and mission specific biases because the data were not calibrated. The main difference between EOT08a and EOT11a are shown in the table 5.

	EOT08a	EOT11a
missions	TOPEX/Poseidon, ERS-1/2, Jason-1, GFO, ENVISAT	TOPEX/Poseidon, Jason-1/2, ERS-2, ENVISAT
mean values	one	mission specific
VCE	no	yes
outlier test	no	yes
IB	old DAC	new DAC
cross-calibration	yes	no
processing	measurement \Rightarrow grid node	grid node \Rightarrow measurement
weighting	depending on depth	depending on signal
composition	no external information	seasonal ice data from NSIDC
tides	$M_2, S_2, N_2, K_2, 2N_2,$ O_1, K_1, Q_1, P_1 M_4	$M_2, S_2, N_2, K_2, 2N_2,$ $O_1, K_1, Q_1, P_1, S_1,$ M_m, M_f, M_4

Table 5: Differences between EOT08a and EOT11a

5 Validation and comparison with other tide models

To validate the EOT11a by means of tidal constants from tide gauges four sets were available. In addition to the three data sets described in the section 2.4 the shallow water data compilation from (R.Ray personal communication 2010) were used for comparisons. We compare the RMS differences between FES2004, EOT08a, GOT4.7, TPXO7.2, EOT10a and EOT11a. Because of different land-ocean-mask and different resolution of the grids the interpolation of the data to the tide gauges stations is not self-evident particularly for the shallow water sites. Therefore any tide constants were excluded from comparisons if the constants couldn't be interpolated for all models to this position. No extrapolation was applied.

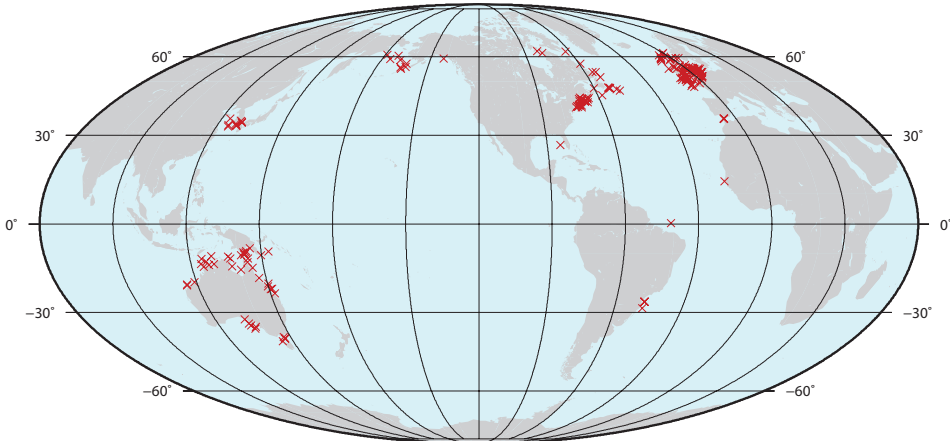


Figure 5: Positions of shallow water tidal constants

The comparison shows that EOT11a performs better than FES2004. The S_2 problem of EOT08a is solved. The EOT11a tends to be better than EOT08a and EOT10a. The well distributed tide gauges of ST102 show that EOT11a is comparable with GOT4.7 and TPXO7.2.

	FES2004	EOT08a	EOT10a	EOT11a	GOT4.7	TPXO7.2	num
M_2	1.45	1.43	1.41	1.42	1.43	1.43	101
S_2	0.86	0.97	0.84	0.84	0.93	0.82	101
N_2	0.67	0.65	0.64	0.64	0.65	0.64	98
K_2	0.49	0.45	0.43	0.46	0.40	0.37	97
K_1	1.01	0.98	0.97	0.96	1.01	1.07	101
O_1	0.75	0.74	0.73	0.73	0.76	0.86	97
P_1	0.41	0.42	0.37	0.37	0.37	0.37	97
Q_1	0.30	0.30	0.27	0.28	0.27	0.27	95

Table 6: Statistic of RMS differences between global tide models and ST102 compilation of tide gauges with known tidal constants

	FES2004	EOT08a	EOT10a	EOT11a	GOT4.7	TPXO7.2	num
M_2	2.61	2.51	2.53	2.51	2.45	2.59	311
S_2	2.09	2.05	2.04	2.02	1.61	1.62	311
N_2	1.02	1.00	1.00	1.01	0.95	0.94	305
K_2	0.97	0.88	0.93	0.89	0.79	0.79	273
K_1	1.90	1.84	1.83	1.82	1.34	1.27	311
O_1	1.51	1.50	1.49	1.45	1.06	1.04	310
P_1	2.84	2.70	2.66	2.60	2.65	2.57	273
Q_1	0.53	0.52	0.48	0.49	0.44	0.44	274

Table 7: Statistic of RMS differences between global tide models and IAPSO compilation of tide gauges with known tidal constants

Although the tidal constants of IAPSO compilation show that TPXO7.2 exhibit the best performance. But the distribution of these tide gauges is not homogeneous and therefore the comparisons with these tidal constants are more or less of local character. The comparisons with WOCE coastal tidal constants are problematic and for the models with the coarse resolution and land-ocean-mask not suitable. These comparisons show that each of EOT tide models performs better than FES2004 for the most tidal constituents. EOT11a exhibits the best statistics. The S_1 constituent seems to be worse than of FES2004, what can be explained with the variability of its tide constants, high correlation with mean values of ESA missions, and possible problems in the altimetric parameters obtained from the air pressure maps. The long period tides are too weak to be well detected from altimeter data therefore there is no significant improvement to FES2004 grids. The long period tides are anyway reliably described by equilibrium theory. The comparisons with shallow water tidal constants shows that both EOT11a and GOT4.7 have the best agreement for three tides. The best three tides belong to TPXO7.2. The K_1 tide from EOT08a exhibits the best comparison results.

The next validation procedure often used for the validation of tide models it is the variance reductions tests of the differences of sea surface heights at the crossover points. The tides cause the differences between ascending and descending tracks at crossover points. Therefore the use of tide model of the better performance should lead to the smaller crossover differences.

	FES2004	EOT08a	EOT10a	EOT11a	num
M_2	11.70	12.06	11.85	11.85	158
S_2	4.34	4.36	4.20	4.18	158
N_2	2.53	2.66	2.53	2.57	158
K_2	1.63	1.52	1.51	1.48	156
$2N_2$	0.53	0.55	0.53	0.53	158
K_1	4.20	4.02	4.02	3.95	158
O_1	3.02	2.97	2.98	2.91	158
P_1	1.37	1.32	1.30	1.31	158
Q_1	0.68	0.62	0.68	0.68	158
S_1	0.38		0.44	0.44	156
M_4	1.47	1.34	1.23	1.27	158
M_m	0.86		0.87	0.87	158
M_f	0.74		0.74	0.74	158

Table 8: Statistic of RMS differences between global tide models and WOCE compilation of tide gauges with known tidal constants

	FES2004	EOT08a	EOT10a	EOT11a	GOT4.7	TPXO7.2	num
M_2	7.54	6.80	6.78	6.31	6.07	6.94	177
S_2	4.84	4.12	4.01	3.95	3.38	3.80	177
N_2	2.67	2.19	2.33	2.09	2.06	2.08	174
K_2	2.20	1.54	1.55	1.37	1.64	1.67	97
K_1	1.88	1.63	1.65	1.66	1.65	1.76	177
O_1	1.31	1.24	1.24	1.45	1.30	1.14	177
P_1	1.08	0.81	0.91	0.79	0.95	0.97	98
Q_1	0.94	0.87	0.83	0.82	0.85	1.08	140
M_4	4.23	2.29	2.67	2.61	2.33	1.88	129

Table 9: Statistic of RMS differences between global tide models and shallow water compilation of tide gauges with known tidal constants

The worse models can't correct the full tidal signal therefore the crossover differences become large. The comparison of crossover statistics should give the information of performance of tide models. There are some weaknesses of these tests. First, the tides are only a part of the sea surface variability therefore the use of the better tide model doesn't lead to improvement of crossover statistic automatically. Second, the empirical tide models were obtained from altimeter data and therefore this kind of tests based on not really independent data. Either completely the same data were used or these data sets were obtained from the same corrections as for the analysis. As example the uncertainties in the dynamic atmospheric corrections can affect the tide modeling and aren't seen in the crossover statistics. Nevertheless these tests provide generally information about regions of improvements or degradation of tide models.

The validation of the tide models by means of crossover statistics was done in the following steps. First, four sets of sea level anomalies were built using the FES2004, EOT08a, EOT10a,

and EOT11a. Second, the crossover differences were computed. Afterwards the variances were computed for grid cells described by means of a regular grid with the resolution of 3° . Because the EOT11a was validated the reductions of variances of this model w.r.t. the other model was computed by means of the following formula:

$$\Delta\sigma_{xo} = \sigma_{xo}^{tm} - \sigma_{xo}^{EOT11a} \quad (22)$$

where σ_{xo}^{EOT11a} variances of crossover differences if EOT11a was used. σ_{xo}^{tm} stands for other tide models. $\Delta\sigma_{xo}$ is the variance reduction should be positive if the EOT11a perform better.

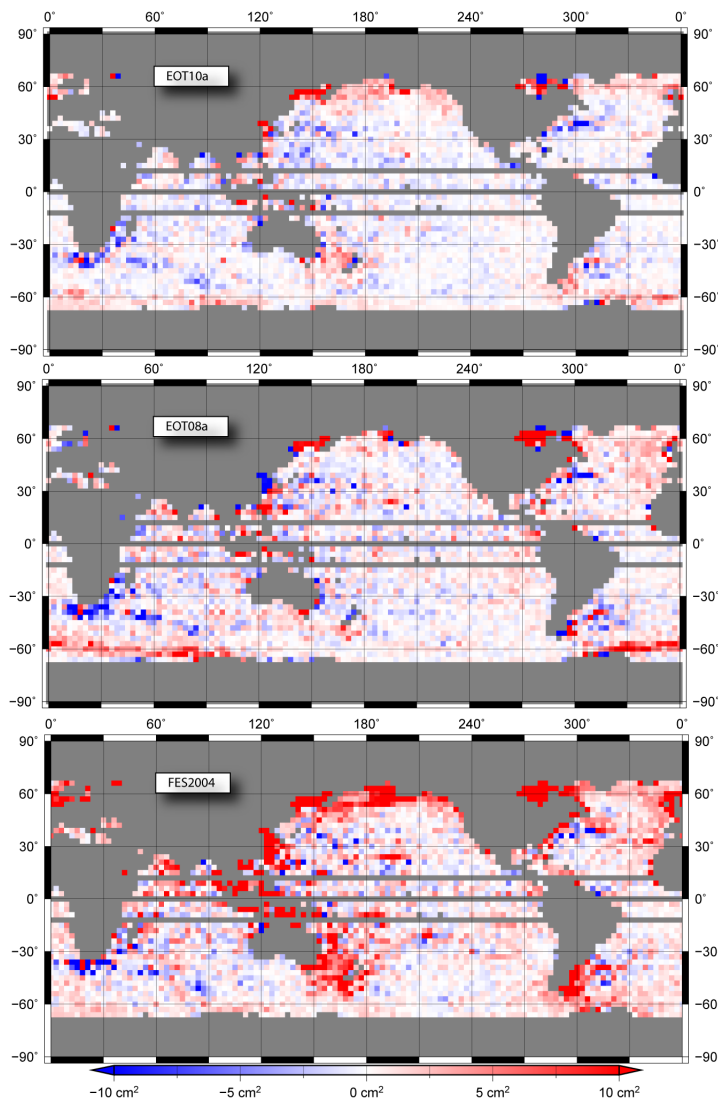


Figure 6: Variance reductions at the crossover points of Jason-1 mission

The figure 6 shows the variance reduction of the crossover points of Jason-1 mission. The high accuracy and short repeat period of this mission allows obtaining the most significant statistics. EOT11a has the best performance in the polar regions. There are no problems available at the seasonal ice boundaries presented in EOT08a. The tides in the Hudson Bay are best described by means of EOT11a. The some degradation of accuracy compared to EOT08a in such regions

as Yellow sea can be explained by the abdication of the cross-calibration. Compared to FES2004 and EOT10a the EOT11a has the best performance in shallow water regions. The statistic in the regions with high sea surface variance is problematical and therefore some rise of variance cannot be explained only by the accuracy of the tide model.

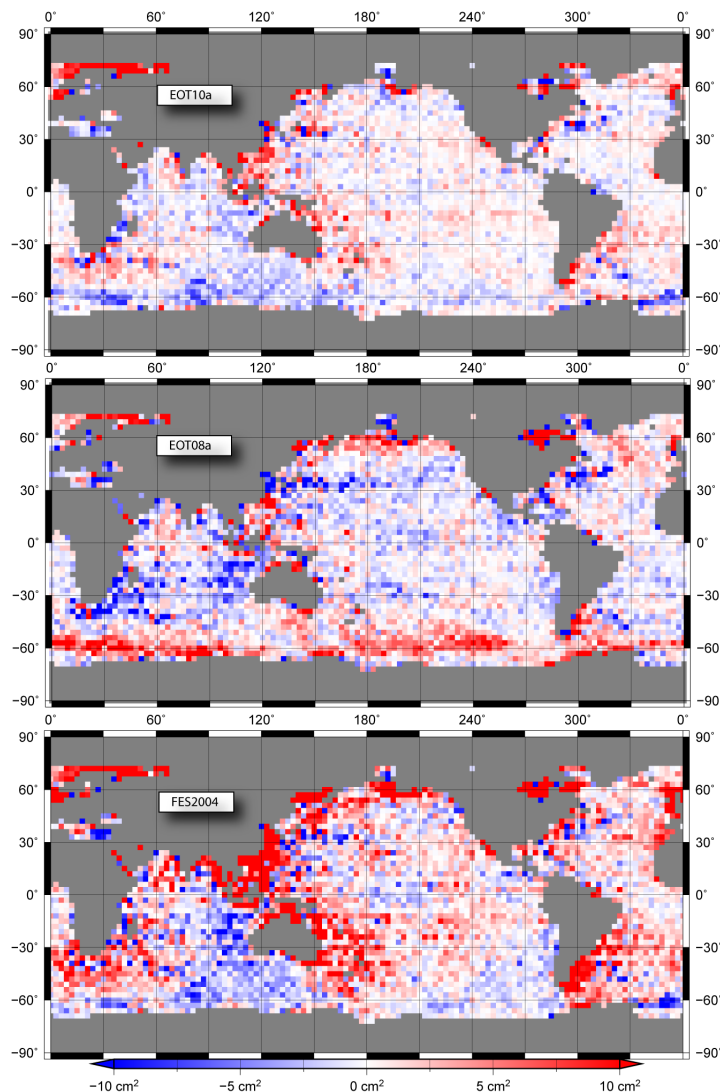


Figure 7: Variance reduction at the crossover points of GFO mission

The statistics of crossover differences of GFO mission shown in figure 7 suffer from low accuracy of orbits. Therefore these statistics should be considered very carefully. The main advantage of the use of these data for validation is the independence of the data because these data weren't used for the composition of EOT11a. According to GFO statistics EOT11a performs better than EOT08a in all polar regions. This model shows the good performance in the north polar regions. EOT11a is the best model for the shallow water regions except of Yellow Sea where EOT08a is the best.

The validation by means of ENVISAT data is more problematical because the effect of solar tides cannot be seen in the statistics. The figure 8 shows that EOT11a is the best tide model. EOT08a performs better in some shallow water regions. Some problems along tracks of this

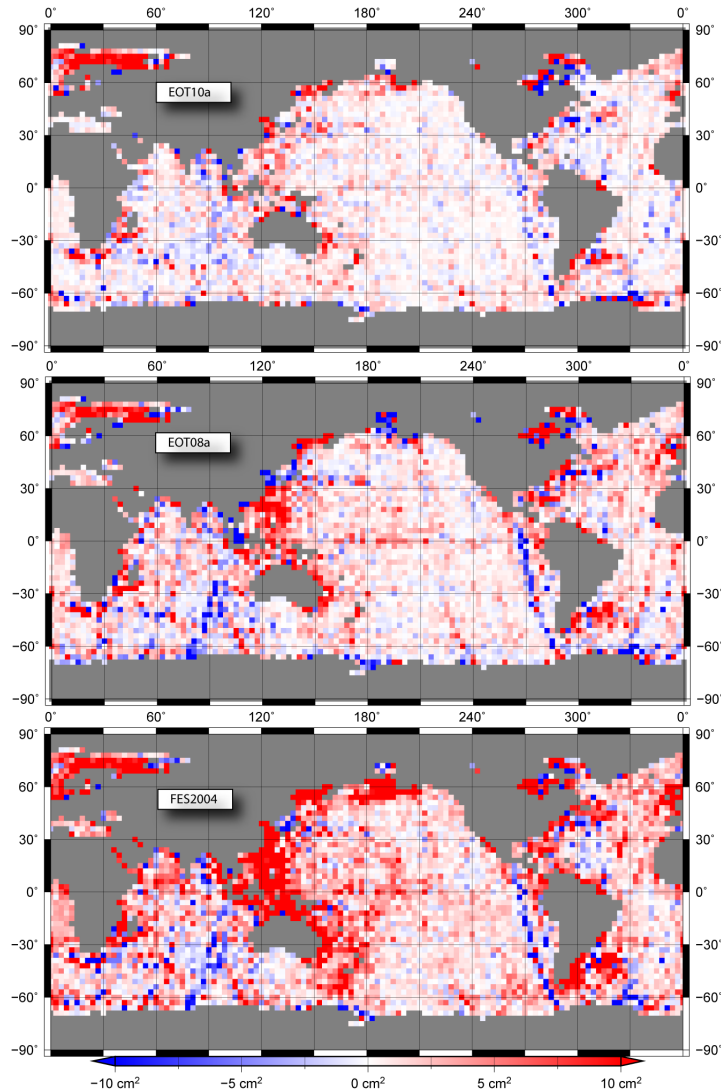


Figure 8: Variance reduction at the crossover points of ENVISAT mission

mission can be explained by the data quality.

6 Conclusions

The long time series of altimeter data were used to empirically estimate a new global tide model, EOT11a. Harmonic analysis was performed for the nodes of a regular grid. By combining carefully pre-processed altimeter systems with different sampling characteristics the severe alias problems for the time series of ERS and ENVISAT could be sufficiently mitigated. The abdication of cross-calibration was necessary because of aliased tidal signals in the time series of available radial error components but leads to worse estimation of tides in shallow water regions. Therefore for the future work the radial error components will be corrected if no signals in the tidal band will be available.

For the most dominant tidal constituents residual tide signals were identified with the amplitudes of up to 15 cm. Because of large weighting parameters is EOT11a a very smooth over open ocean therefore for the most tidal signals the large scale pattern with the amplitudes of 1-2 cm were identified. Some experiments with considerable smaller weighting parameters shows that in the open ocean the small scale pattern available which are the surface manifestation of baroclinic tides. Therefore the future EOT model will consists of baroclinic tidal parts which will be considered separately. The problem with the solar tides has been solved what could be proven by means of comparison with the tidal constants obtained from tide gauges. The long period tides and S_1 tidal constituent exhibit large scale pattern in some regions but could not really validated because of absence of independent data sources.

References

- Andersen 1999** ANDERSEN, O.B.: Shallow water tides in the noethwest European shelf region from TOPEX/Poseidon altimetry. In: *J. Geophys. Res.* 104 (C4) (1999), S. 7729–7741
- Cartwright und Ray 1991** CARTWRIGHT, D.E. ; RAY, R.D.: Energetic of global ocean tides from Geosat altimetry. In: *J. Geophys. Res.* 96(C9) (1991), S. 16,897–19.912
- Cartwright 1990** CARTWRIGHT, D.E. R.D. R.: Oceanic tides from Geosat Altimetry. In: *J. Geophys. Res.* 95(C3) (1990), S. 3096–3090
- Chambers u. a. 2003** CHAMBERS, D. P. ; HAYES, S. A. ; RIES, J. C. ; URBAN, T. J.: New TOPEX sea state bias models and their effect on global mean sea level. In: *J. Geophys. Res.* 108(C10) (2003)
- Desai und Wahr 1995** DESAI, Sh.D. ; WAHR, J.M.: Empirical ocean tide models estimated from TOPEX/Poseidon altimetry. In: *J. Geophys. Res.* 100(C12) (1995), S. 25,205–25,228
- Eanes 1994** EANES, R. J.: Diurnal and semidiurnal tides from TOPEX/POSEIDON altimetry. In: *Eos Trans, AGU* 76(16) (1994), Nr. 108
- Egbert 2010** EGBERT, G.: *TPXO7.2*. 2010. – URL <http://volkov.oce.orst.edu/tides/>
- Egbert und Erofeeva 2002** EGBERT, G. D. ; EROFEEVA, S. Y.: Efficient inverse modelling of barotropic ocean tides. In: *J. Atmos. Oceanic Technol.* 12 (2002), Nr. 2, S. 183–204
- Eicker 2008** EICKER, Annette: *Gravity field refinement by radial basis functions from in-situ satellite data*, Institut für Geodäsie und Geoinformation, Universität Bonn, Dissertation, 2008
- Eymard u. a. 2003** EYMARD, L. ; OBLIGES, E. ; 2003 N. TRAN: ERS2/ MWR drift evaluation and correction / CLS. 2003. – CLS.DOS/NT/03.688
- F. Lyard u. a. 2006** F. LYARD ; F. LEFEVRE ; T. LETELLIER ; FRANCIS, O.: Modelling the global ocean tides: modern insights from FES2004. In: *Ocean Dynamics* (2006), Nr. 56, S. 394–415
- Farrell 1972** FARRELL, W.E.: Deformation of Earth by surface loads. In: *Reviews of Geophysics and Space Physics* 10 (1972), Nr. 3, S. 761–797
- Han u. a. 2005** HAN, S. C. ; SHUM, C. K. ; MATSUMOTO, K.: GRACE observations of M2 and S2 ocean tides underneath the Filchner-Ronne and Larsen ice shelves. In: *Geophys. Res. Let* 32 (2005)
- Hernandez und Schaeffer 2000** HERNANDEZ, F. ; SCHAEFFER, P.: Altimetric Mean Sea Surfaces and Gravity Anomaly maps inter-comparisons / CLS Ramonville St Agne. 2000. – AVI-NT-011-5242-CLS
- King und Padman 2005** KING, Matt A. ; PADMAN, Laurie: Accuracy assessment of ocean tide models around Antarctica. In: *Geophys. Res. Let* 32 (2005), S. L23608
- Knudsen 2002** KNUDSEN, P.: Correcting GRACE gravity fields for ocean tide effects. In: *Geophys. Res. Let* 29 (2002), Nr. 8

- L. Carrère und Lyard 2003** L. CARRÈRE ; LYARD, F.: Modeling the barotropic response of the global ocean to atmospheric wind and pressure forcing—comparisons with observations. In: *Geophys. Res. Let.* 30 (2003), Nr. 6
- Le Provost 2001** LE PROVOST, C.: *Satellite altimetry and earth sciences: a handbook of techniques and applications*. Kap. Ocean Tides. In: FU, Lee-Lueng (Hrsg.) ; CAZENAVE, Anny (Hrsg.): *Satellite Altimetry and Earth Sciences*, Academic Press, 2001
- Le Provost 2002** LE PROVOST, C: FES2002 – A new version of the FES tidal solution series. In: *Jason-1 Science Working Team Meeting , Abstract Volume, Biarritz, France*, 2002
- Matsumoto u. a. 2000** MATSUMOTO, K. ; T. TAKANEZAWA ; OOE, M.: Ocean tide models developed by assimilating TOPEX/POSEIDON altimeter data into hydrodynamical model: a global model and a regional model around Japan. In: *J. of Oceanography* 56 (2000), S. 567–581
- Ponchant und Lyard 2008** PONCHANT, Frederique ; LYARD, Florent: *Tidal constants. World Ocean Circulation Experiment (WOCE) sea level Data Assembly Centre (DAC)*. Website. 2008. – downloaded in 2008
- Ray 1998** RAY, R. D.: *personnel communication*. 1998
- Ray 1999** RAY, R. D.: A Global Ocean Tide Model from TOPEX/Poseidon Altimetry: GOT99.2 / NASA. 1999. – Forschungsbericht
- Savcenko und W.Bosch 2004** SAVCENKO, R. ; W.BOSCH: *Shallow water tide analysis with complementary tracks of Jason-1 T/PEM*. EGU General Assembly, Nice, France, April 25-30. 2004
- Scharroo und Visser 1998** SCHARROO, R. ; VISSER, P. N. A. M.: Precise orbit determination and gravity field improvement for the ERS satellites. In: *J. Geophys. Res* 103(C4) (1998), S. 8113–8127
- Schrama u. a. 2000** SCHRAMA, E. ; SCHARROO, R. ; NAEIJE, M.: Radar Altimeter Database System (RADS): Towards a generic multi-satellite altimeter database system / CRS/SRON, Delft, The Netherlands. 2000. – USP-2 report 00-11
- Schrama und Ray 1994** SCHRAMA, E.J.O. ; RAY, R.D.: A preliminary tidal analysis of TOPEX/Poseidon altimetry. In: *J. Geophys. Res.* 99(C12) (1994), S. 24,799–24,808
- Shum u. a. 1997** SHUM, C. K. ; WOODWORTH, P. L. ; ANDERSEN, O. B. ; EGBERT, G. D. ; FRANCIS, O. ; KING, C. ; KLOSKO, S. M. ; PROVOST, C. L. ; X. LI ; MOLINES, J-M. ; PARKE, M. E. ; RAY, R. D. ; SCHLAX, M. G. ; STAMMER, D. ; TAPLEY, C. C. ; VINCENT, P. ; WUNSCH, C. I.: Accuracy assessment of recent ocean tide models. In: *J. Geophys. Res.* 102 (C11) (1997), S. 25,173–25,194
- Smith 1999** SMITH, A.J.E.: *Application of satellite altimetry for global ocean tide modelling.*, Institute for Earth-Oriented Space Research. Delft University of technology. Faculty of Aerospace Engineering., Dissertation, 1999
- Smith 2000** SMITH, A.J.E. B.A.C. Ambrosius K.F. W.: Ocean tides from T/P, ERS-1, and GEOSAT altimetry. In: *J. of Geodesy* (2000), Nr. 74, S. 399–413

- Smithson 1992** SMITHSON, M. J.: *Pelagic tidal constants – 3. IAPSO Publications Scientifique No. 35*. Published by the International Association for Physical Sciences of the Ocean (IAPSO) of the International Union of Geodesy and Geophysics. 191pp. 1992
- Wessel und Smith 1996** WESSEL, P. ; SMITH, W. H. F.: A Global Self-consistent, Hierarchical, High-resolution Shoreline Database. In: *J. Geophys. Res* 101 (1996), Nr. B4, S. 8741–8743
- Wünsch u. a. 2005** WÜNSCH, J. ; SCHWINTZER, P. ; PETROVIC, S.: Comparison of two different ocean tide models especially with respect to the GRACE satellite mission / GeoForschungsZentrum Potsdam. 2005. – Scientific Technical Report STR05/08

7 Acknowledgement

We gratefully acknowledge the provision of

- FES2004 model by T. Lettillier,
- the revised version of FES2004 model and DAC by AVISO,
- TPXO7.2 by Gary Egbert,
- GOT4.7 and shallow water tidal constants by Richard Ray,
- DTU10 by Yongcun Cheng and Ole Andersen,
- the DEOS orbits for ESA satellites.

This study has been funded by the Deutsche Forschungsgemeinschaft (DFG) under the grand BO 1228/6-2.

A Appendix

The following appendix provides maps showing the geographical distribution of amplitudes (always top panels) and phases (always bottom panels) for the estimated residuals of all constituents. Zoomed maps are provided for the Patagonian Shelf (A.1), the North-West European Shelf (A.2), and the Yellow Sea (A.3). Section A.4 provides global maps of the residuals.

The 7.5'x7.5' grids of the EOT11a model are available at the anonymous ftp

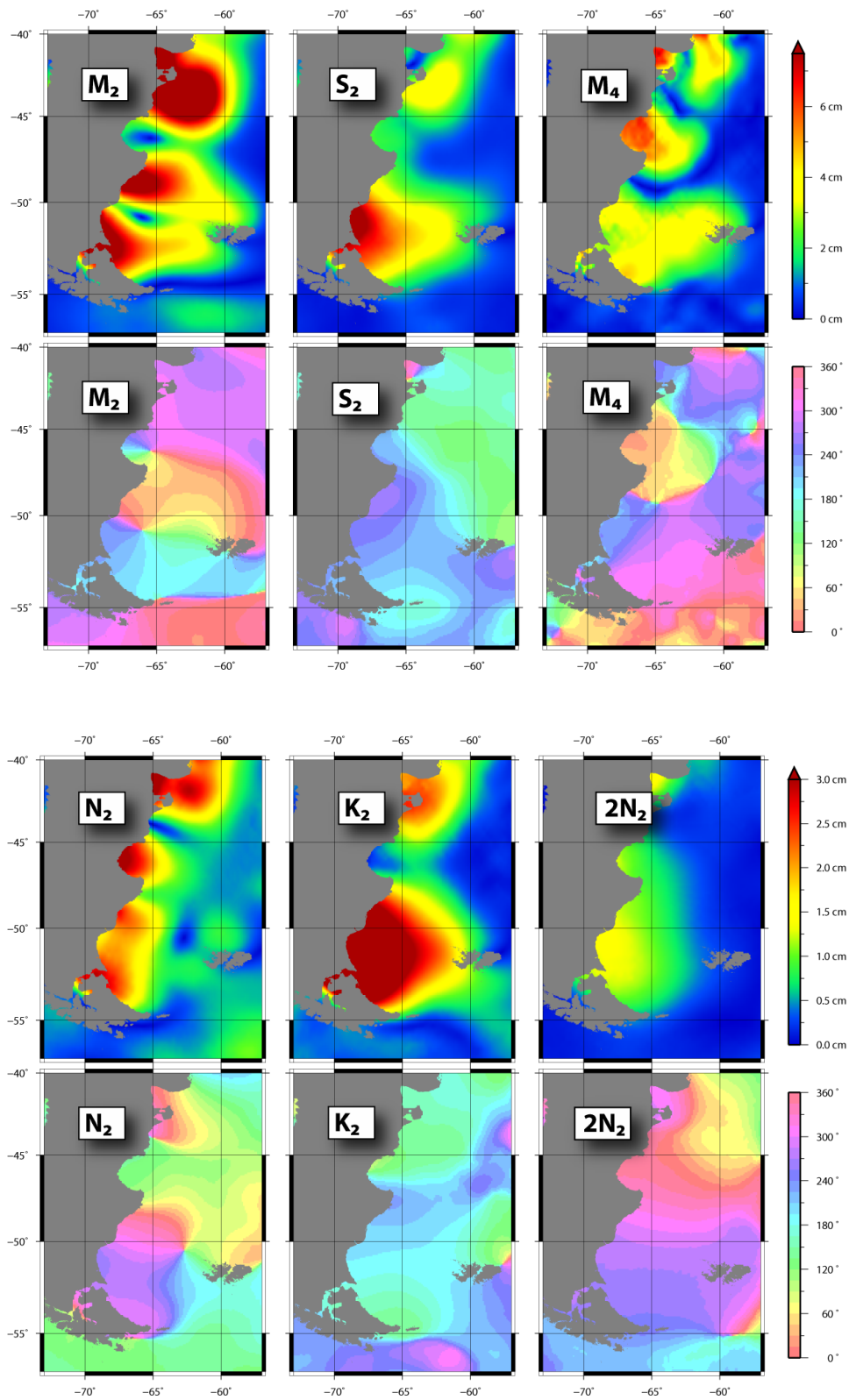
`ftp.dgfi.badw.de`

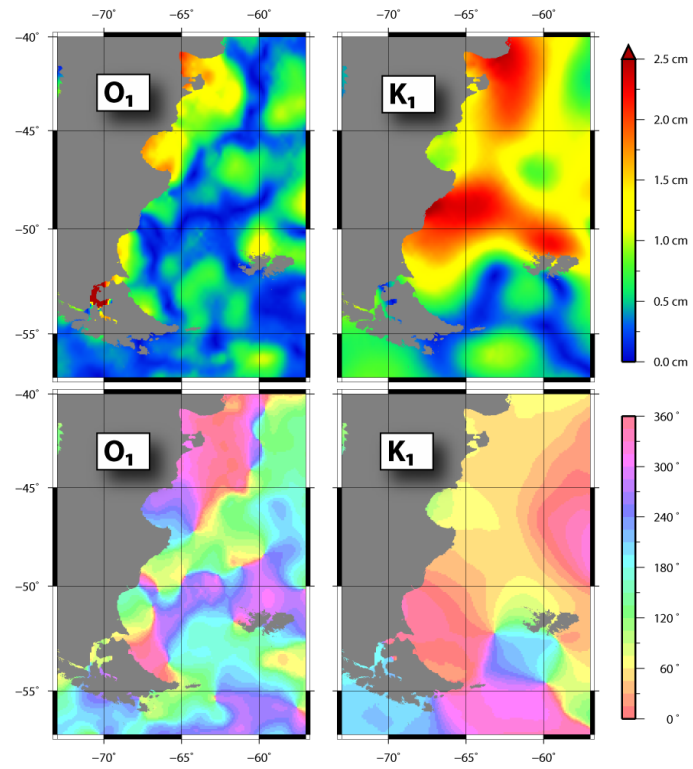
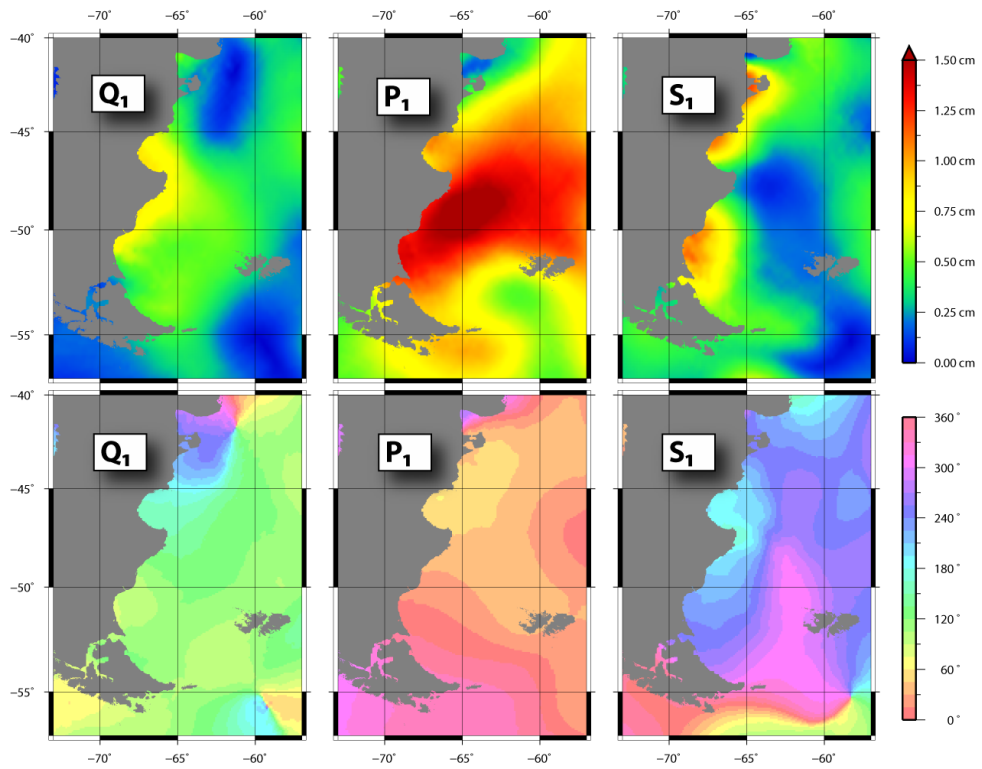
in directory

`pub/EOT11a`

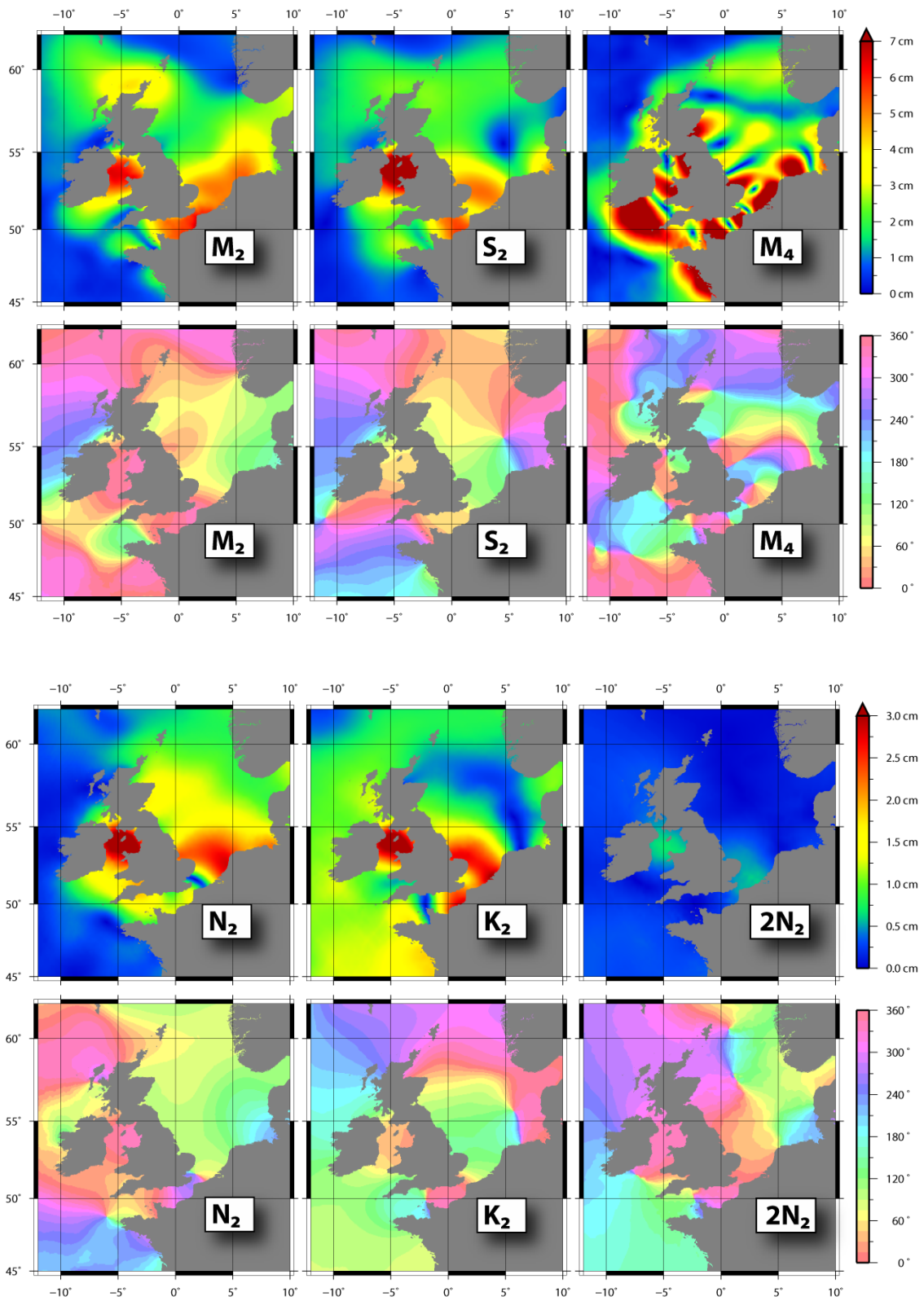
together with the pdf version of this report. The tables are provided in NetCDF format, following the COARDS, version 1.0 standard. NetCDF (network Common Data Form) is a set of software libraries and machine-independent data formats that support the creation, access, and sharing of array-oriented scientific data (see <http://www.unidata.ucar.edu/software/netcdf/> for details). The grids can also be read by the Generic Mapping Tools (GMT), open source software developed and maintained by Paul Wessel and Walter H. F. Smith (see <http://gmt.soest.hawaii.edu/>).

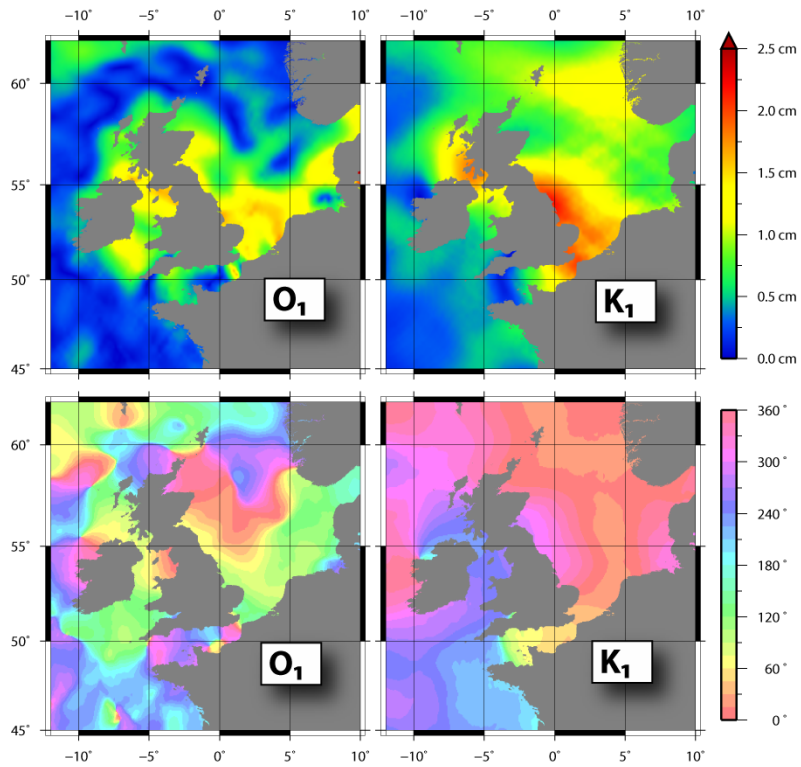
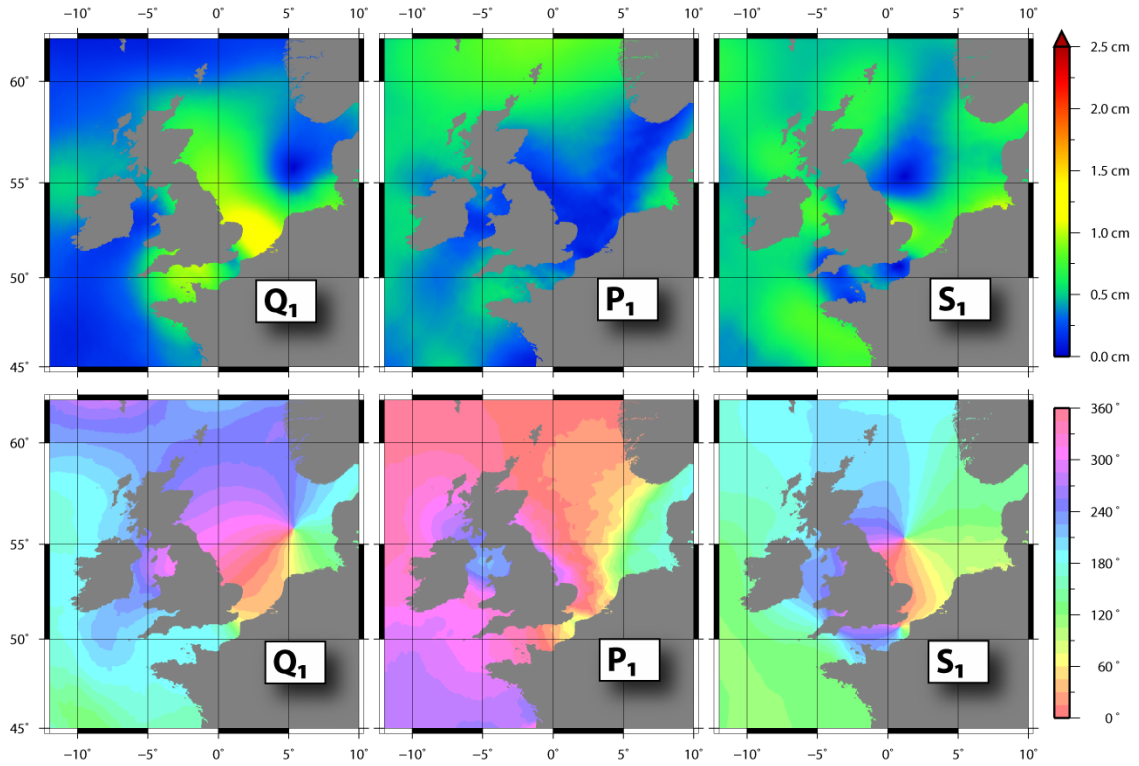
A.1 Patagonian shelf



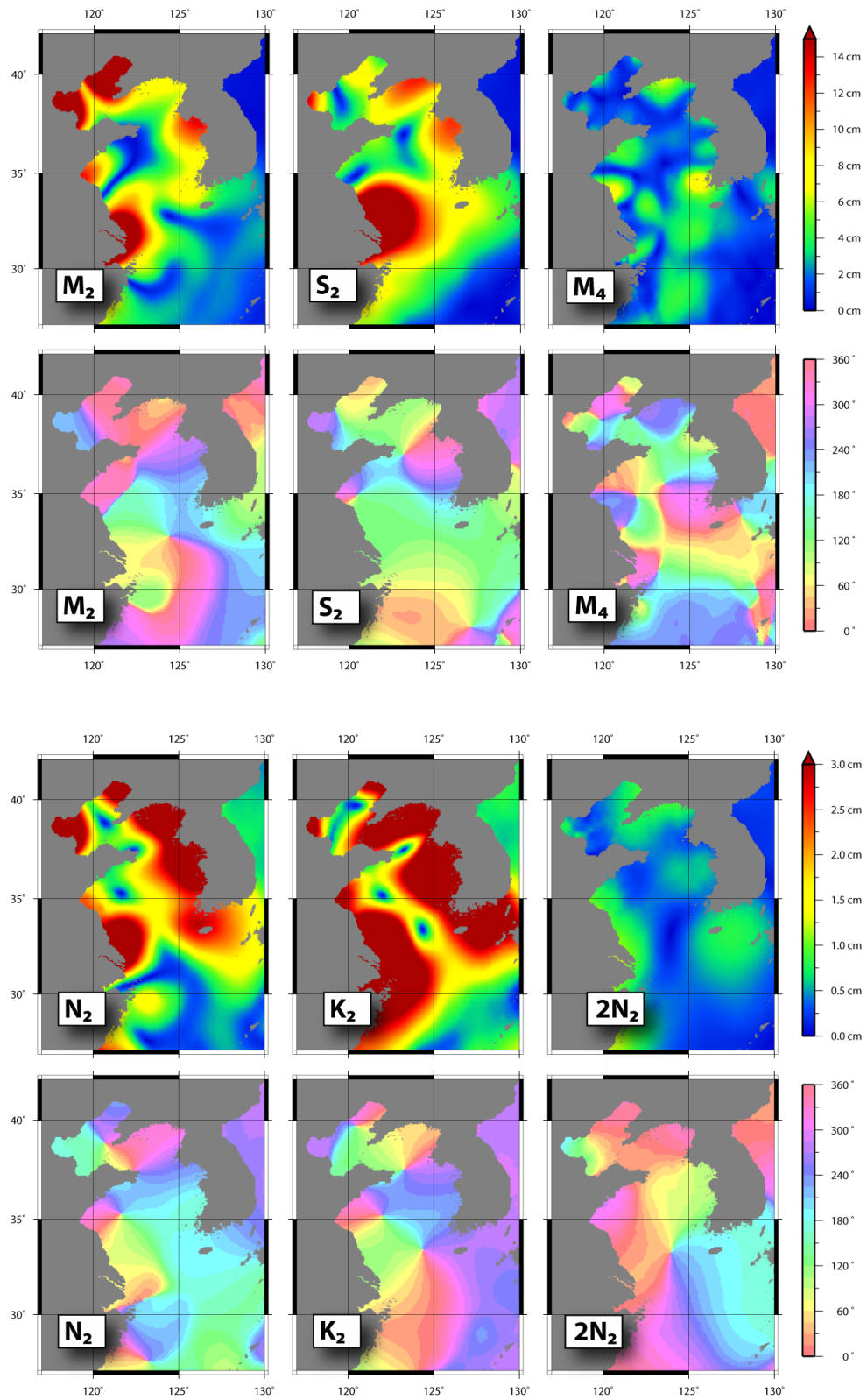


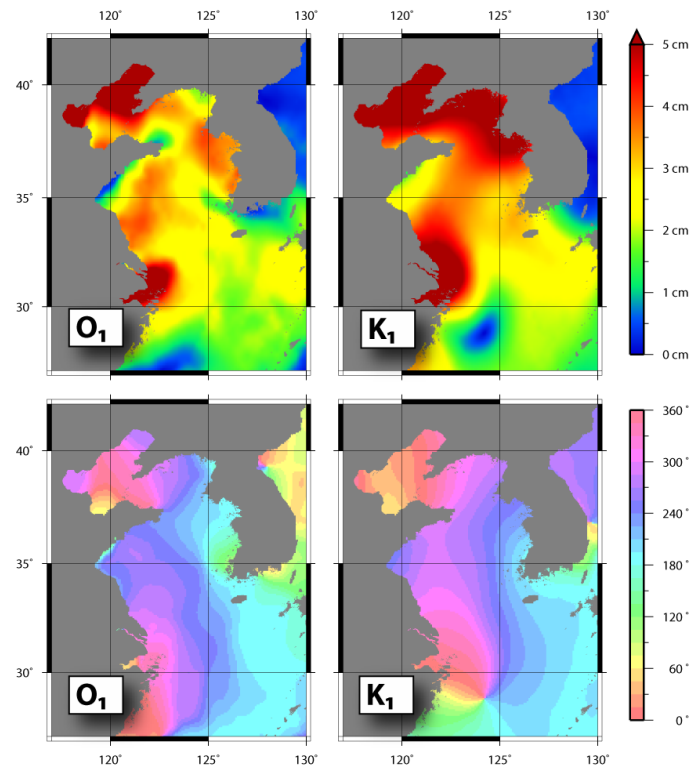
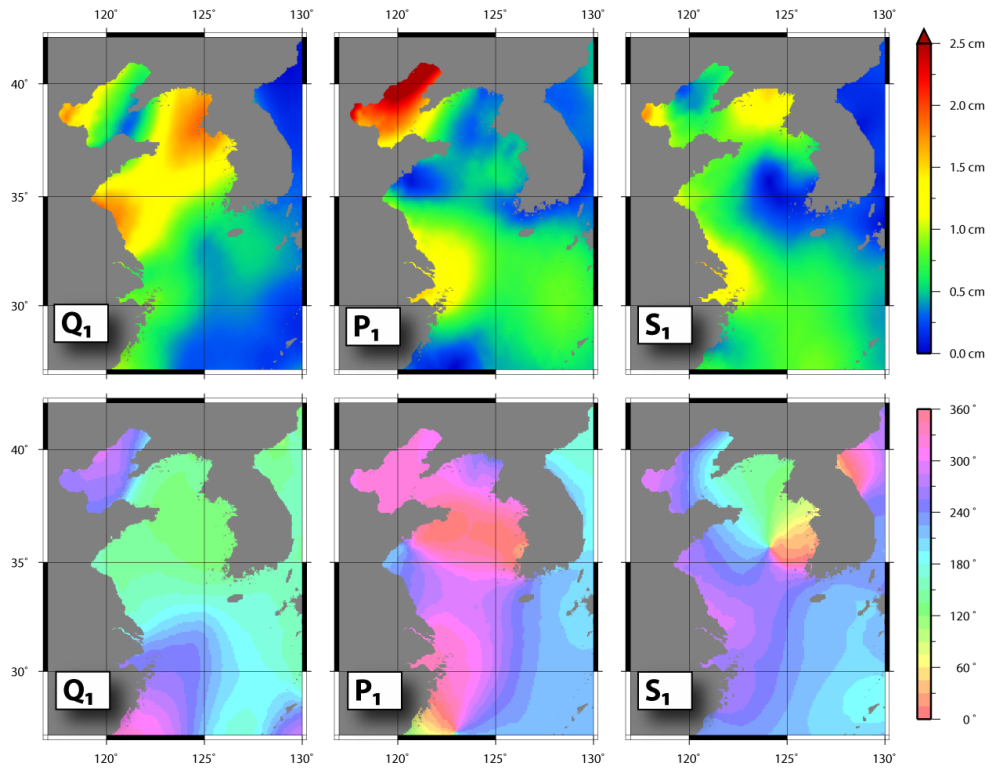
A.2 North-West European Shelf



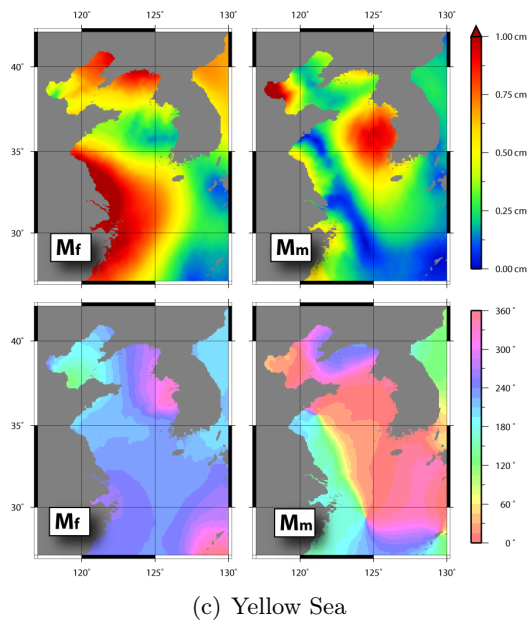
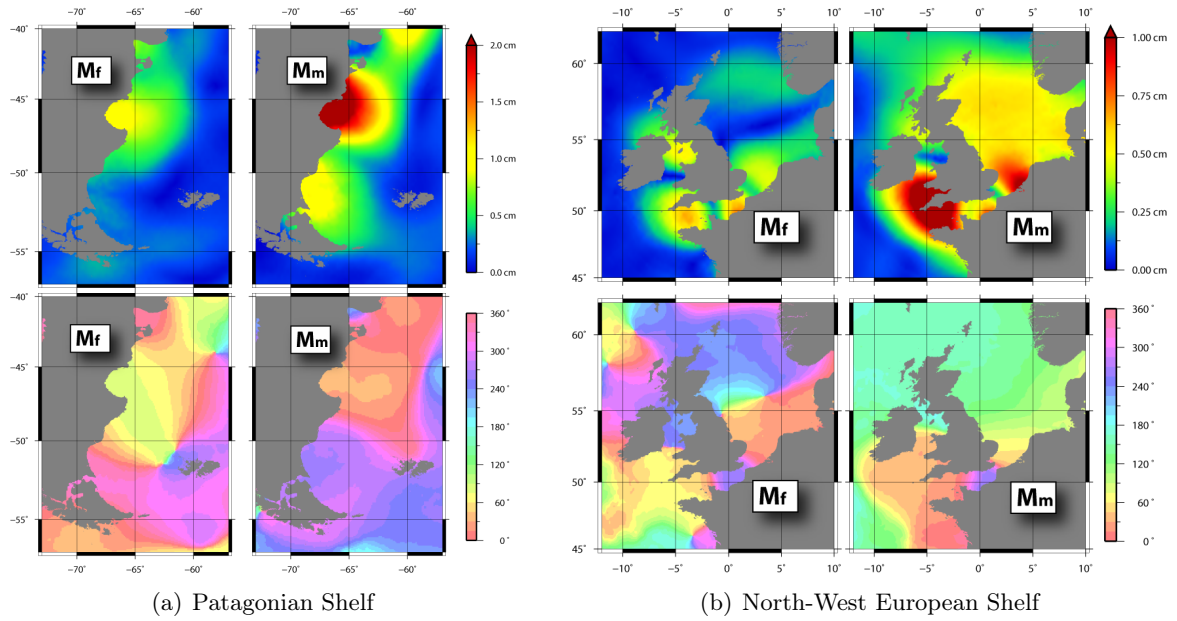


A.3 Yellow Sea





A.4 Long period tides in shallow water areas



A.5 Global Maps

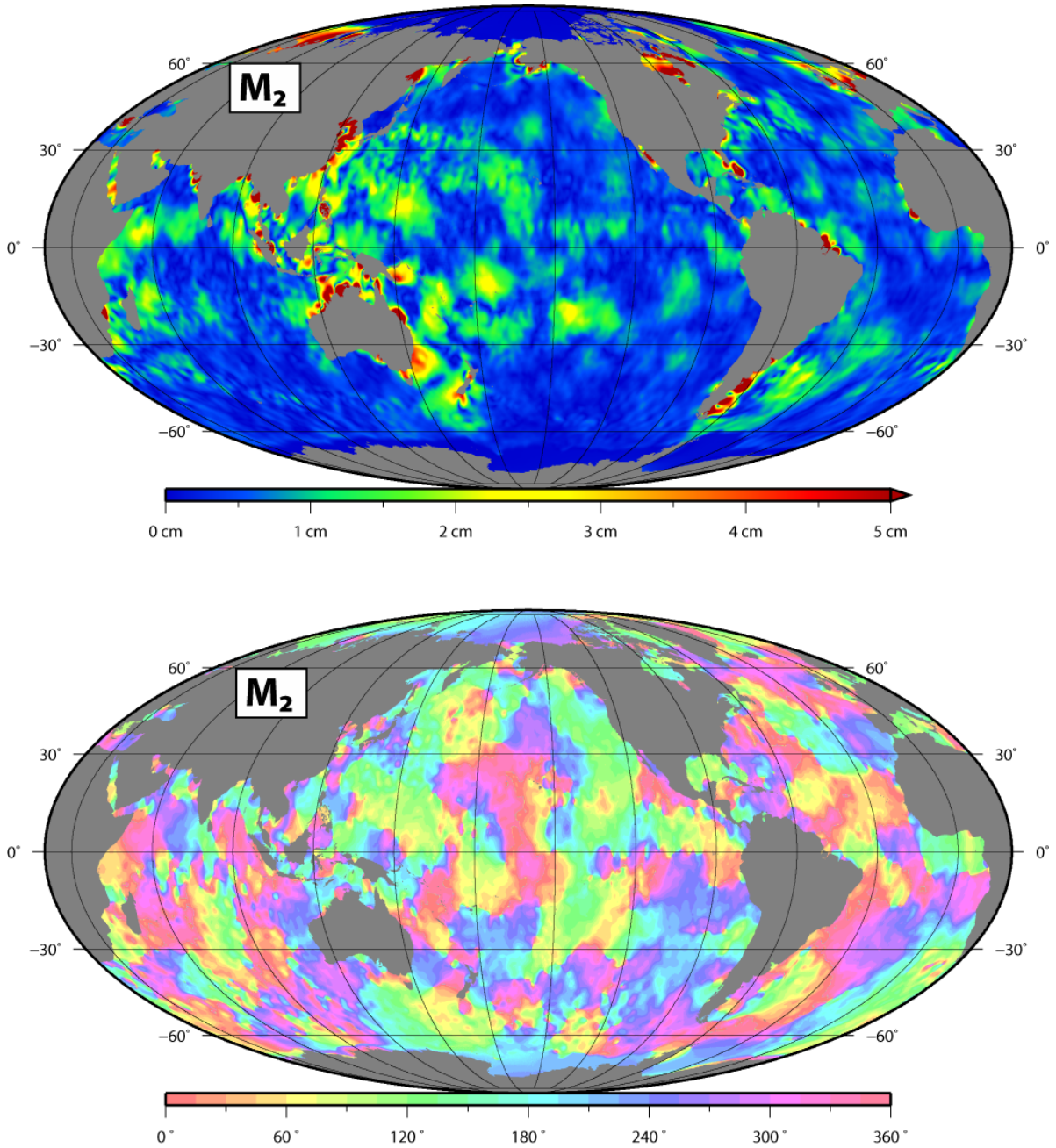


Figure A.1: Residual amplitude of M_2 tidal constituent w.r.t. FES2004

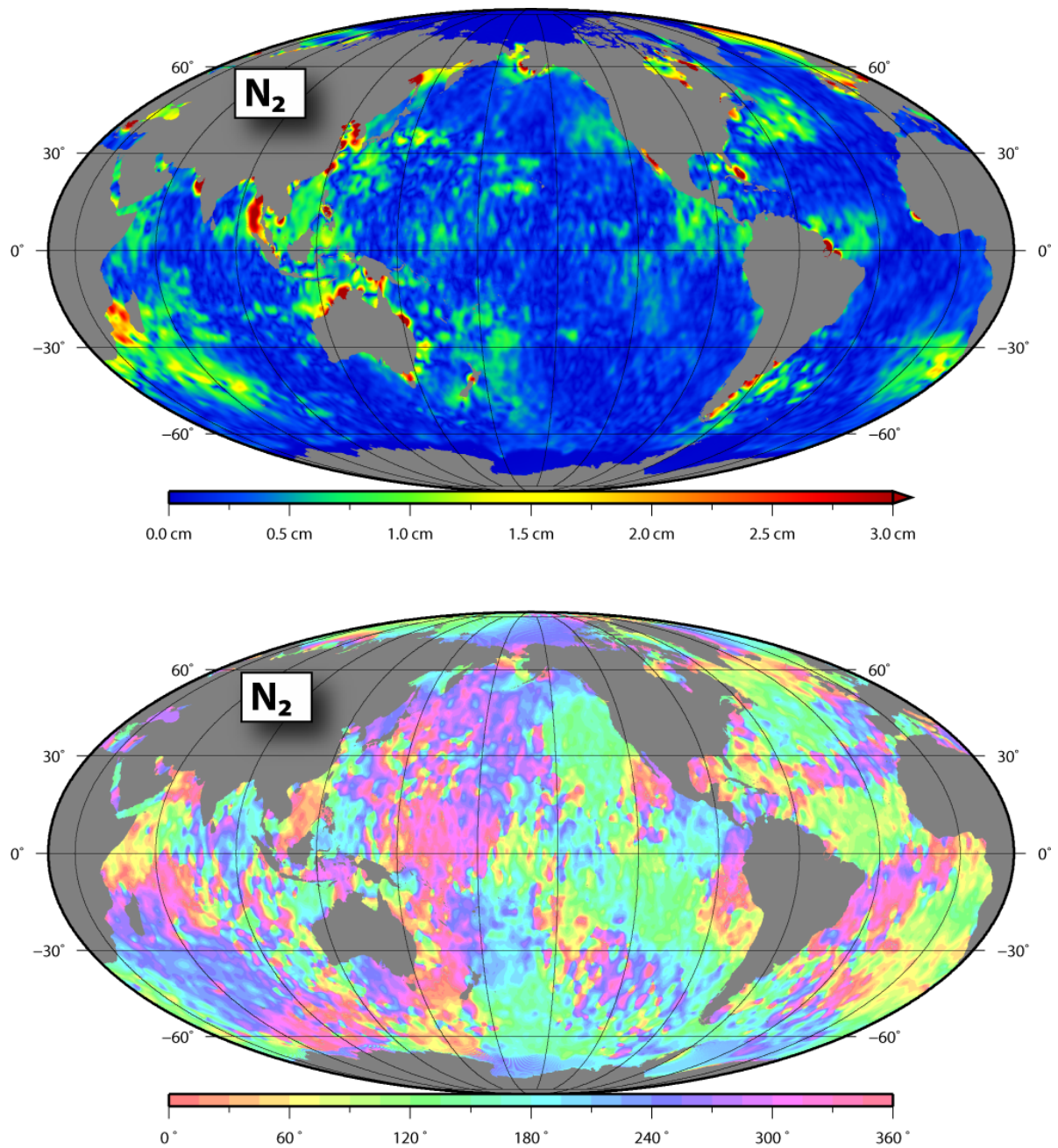


Figure A.2: Residual amplitude of N_2 tidal constituent w.r.t. FES2004

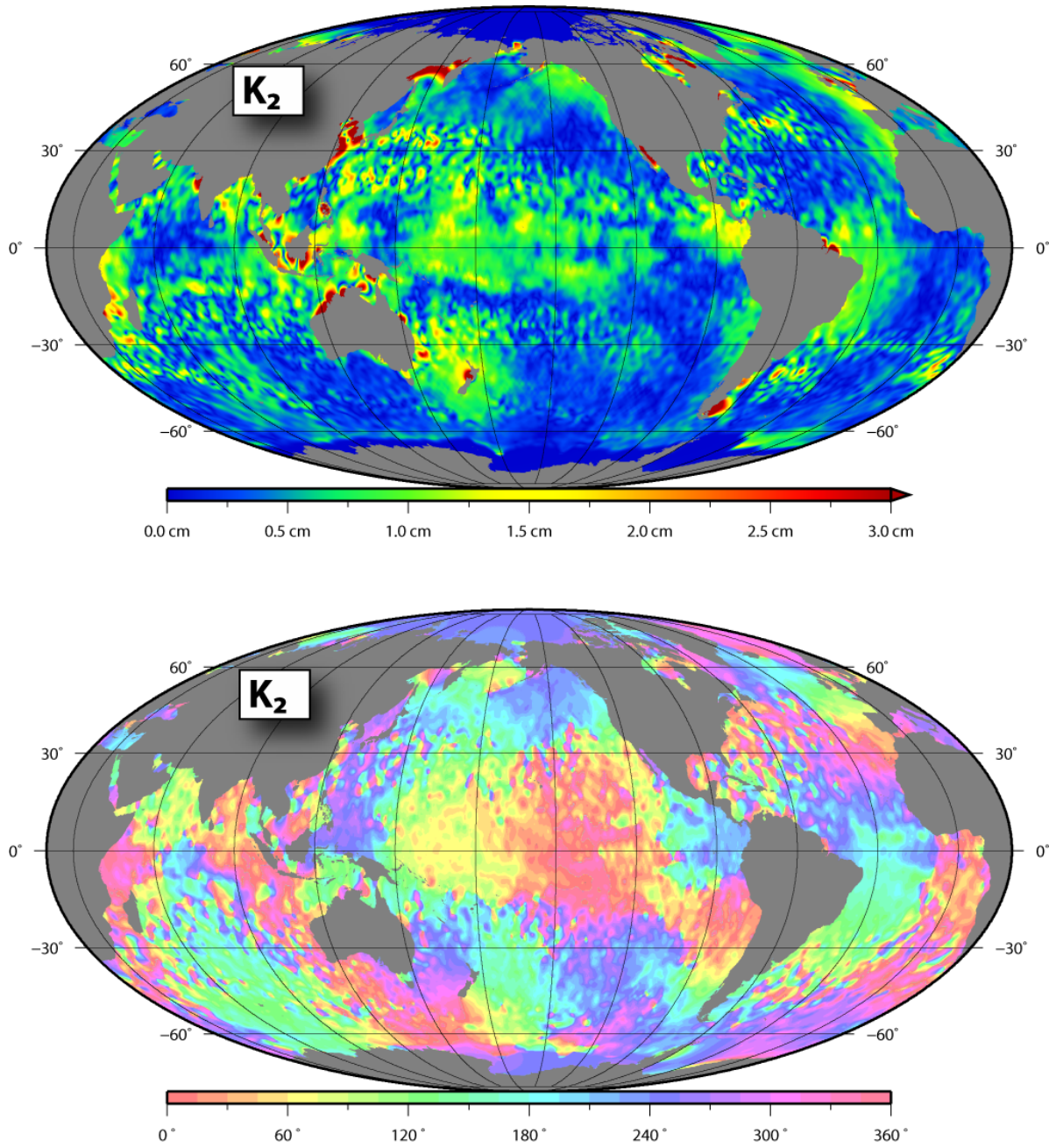


Figure A.3: Residual amplitude of K_2 tidal constituent w.r.t. FES2004

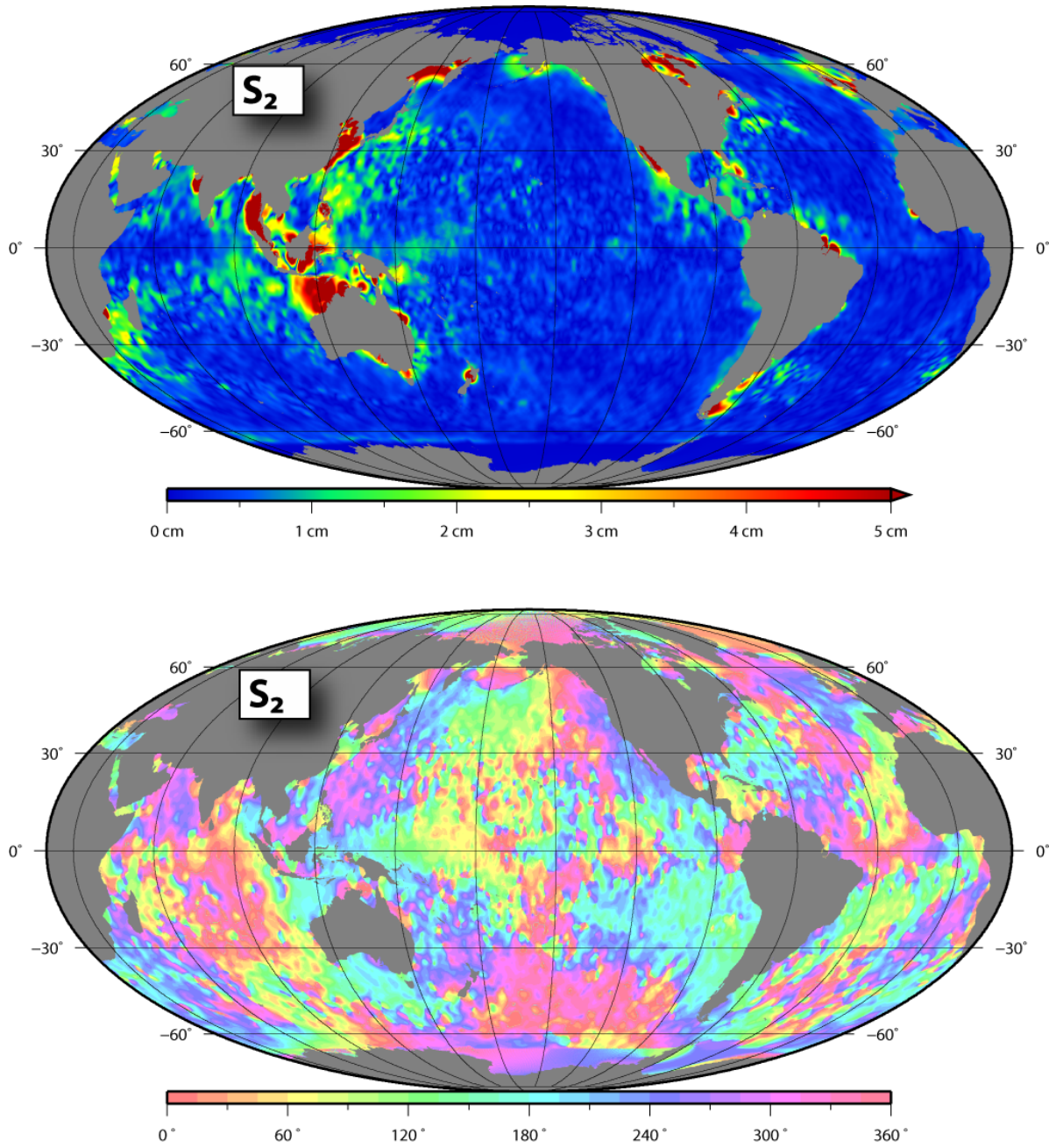


Figure A.4: Residual amplitude of S_2 tidal constituent w.r.t. FES2004

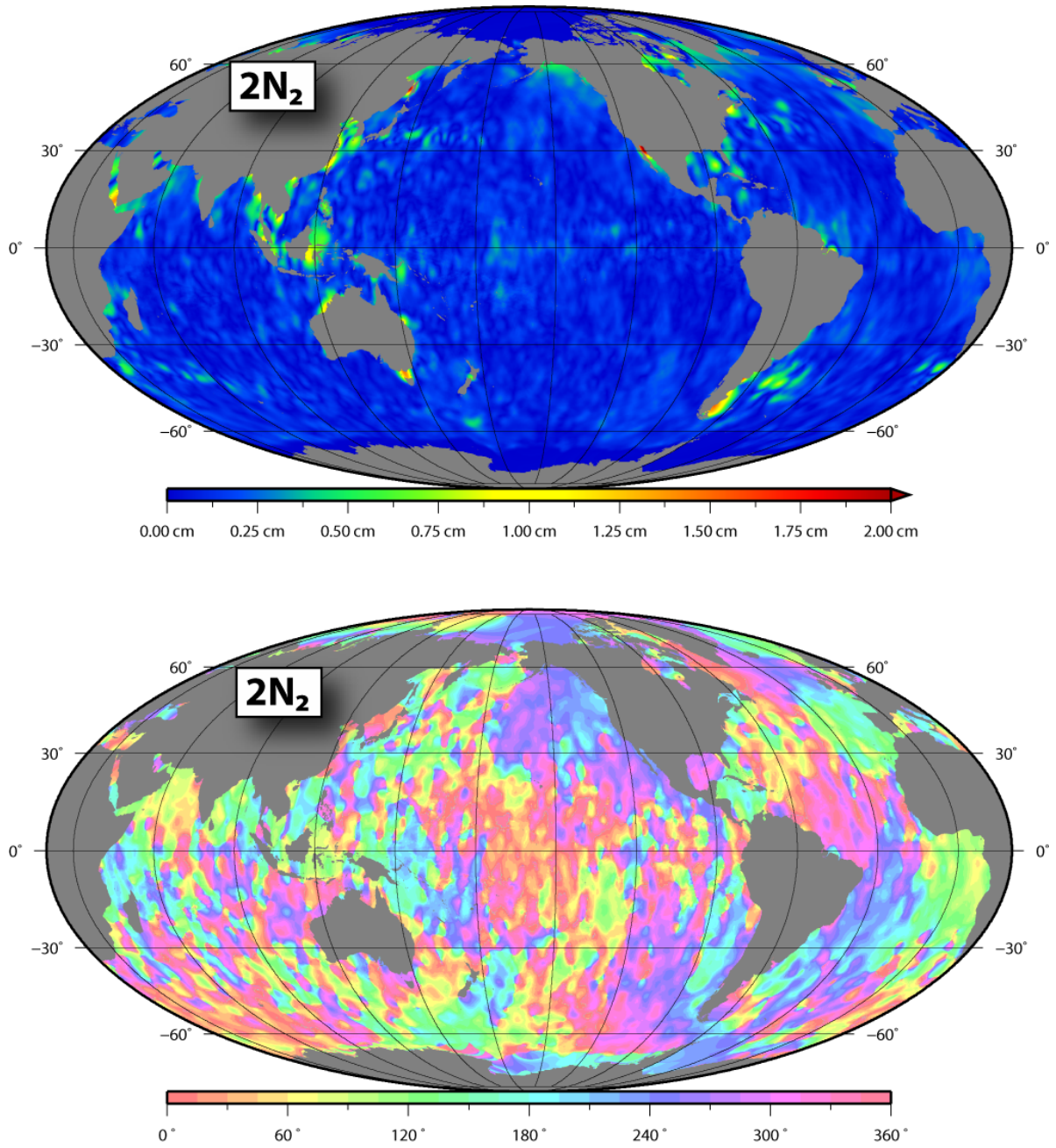


Figure A.5: Residual amplitude of $2N_2$ tidal constituent w.r.t. FES2004

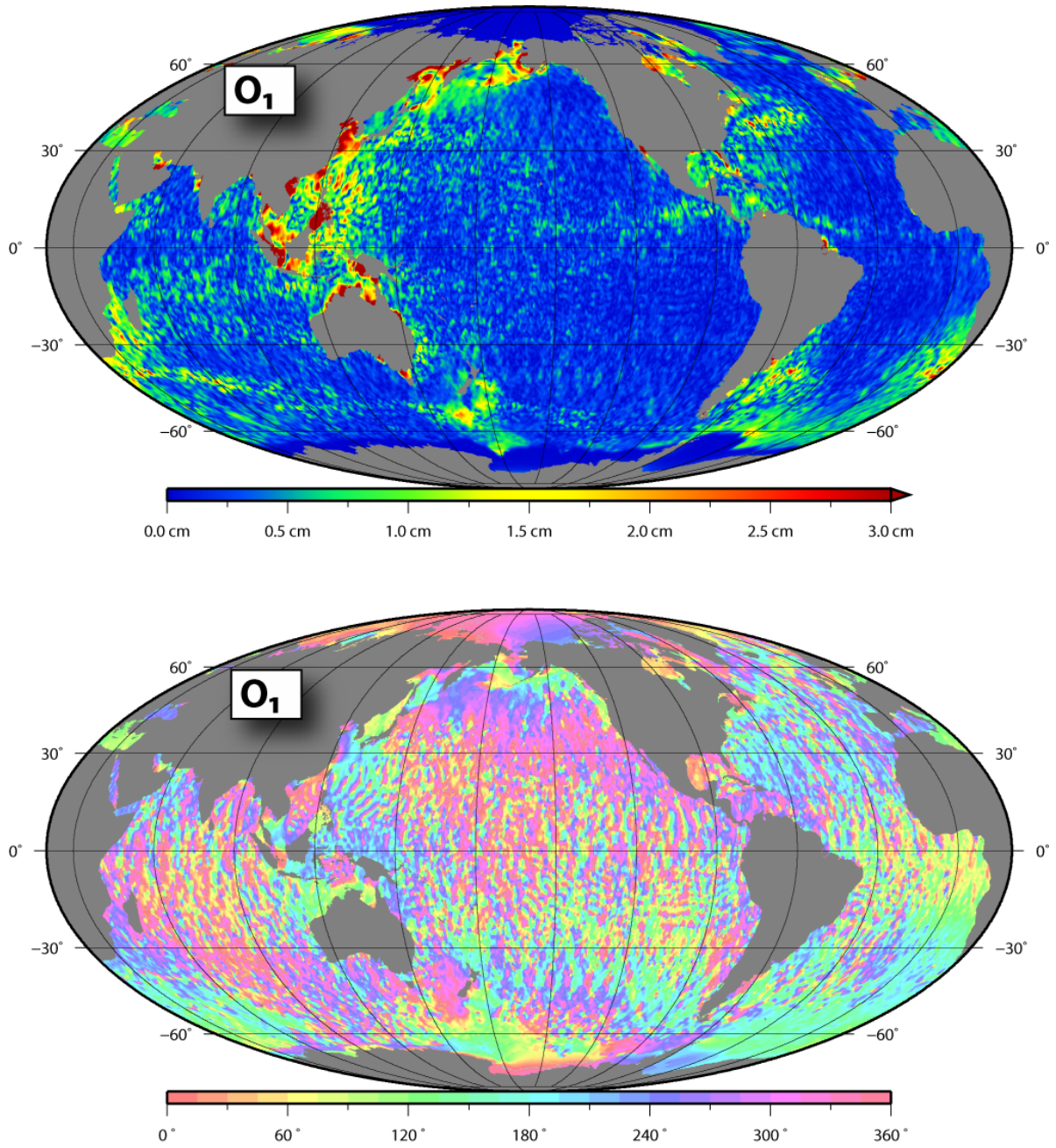


Figure A.6: Residual amplitude of O_1 tidal constituent w.r.t. FES2004

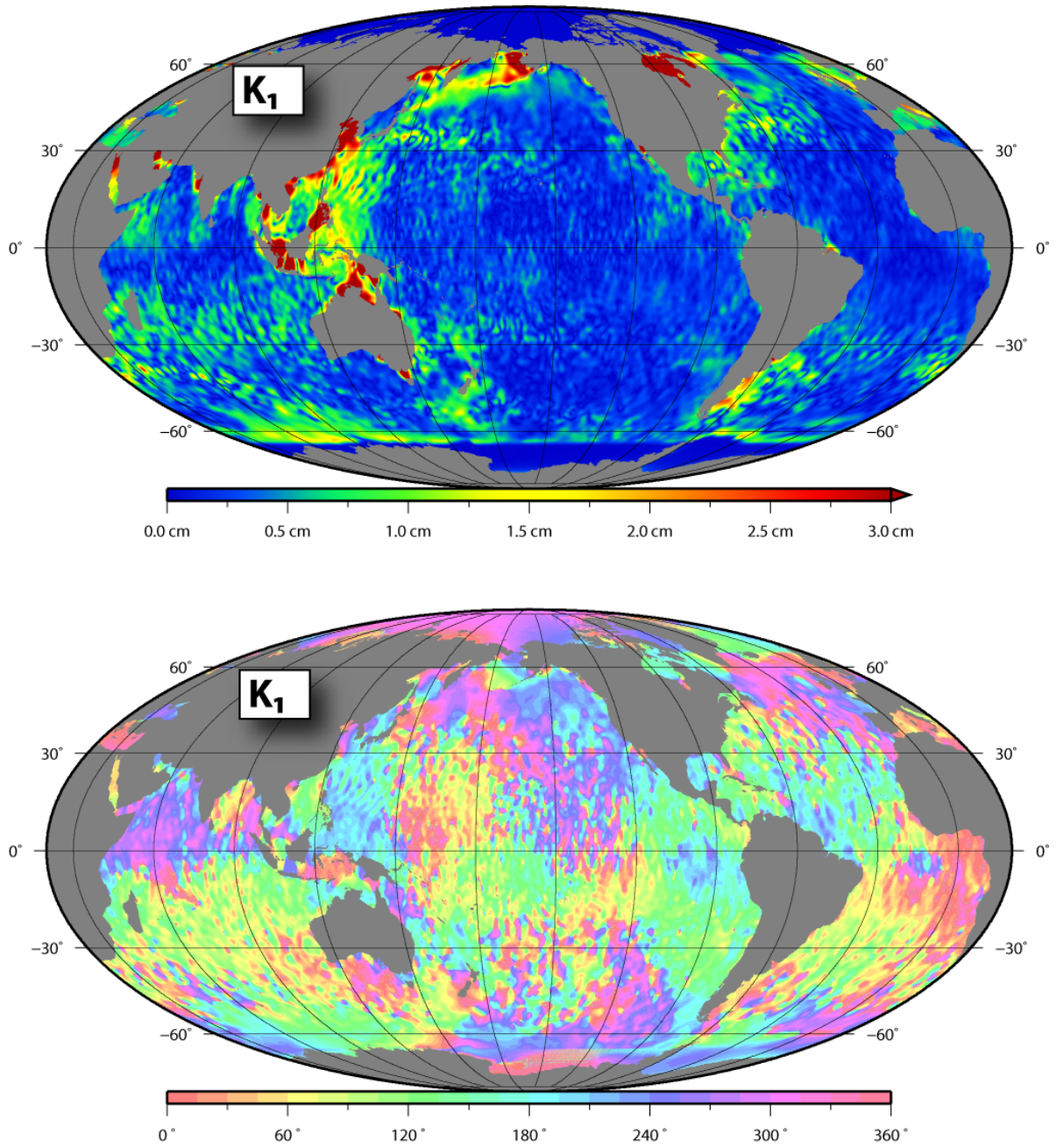


Figure A.7: Residual amplitude of K_1 tidal constituent w.r.t. FES2004

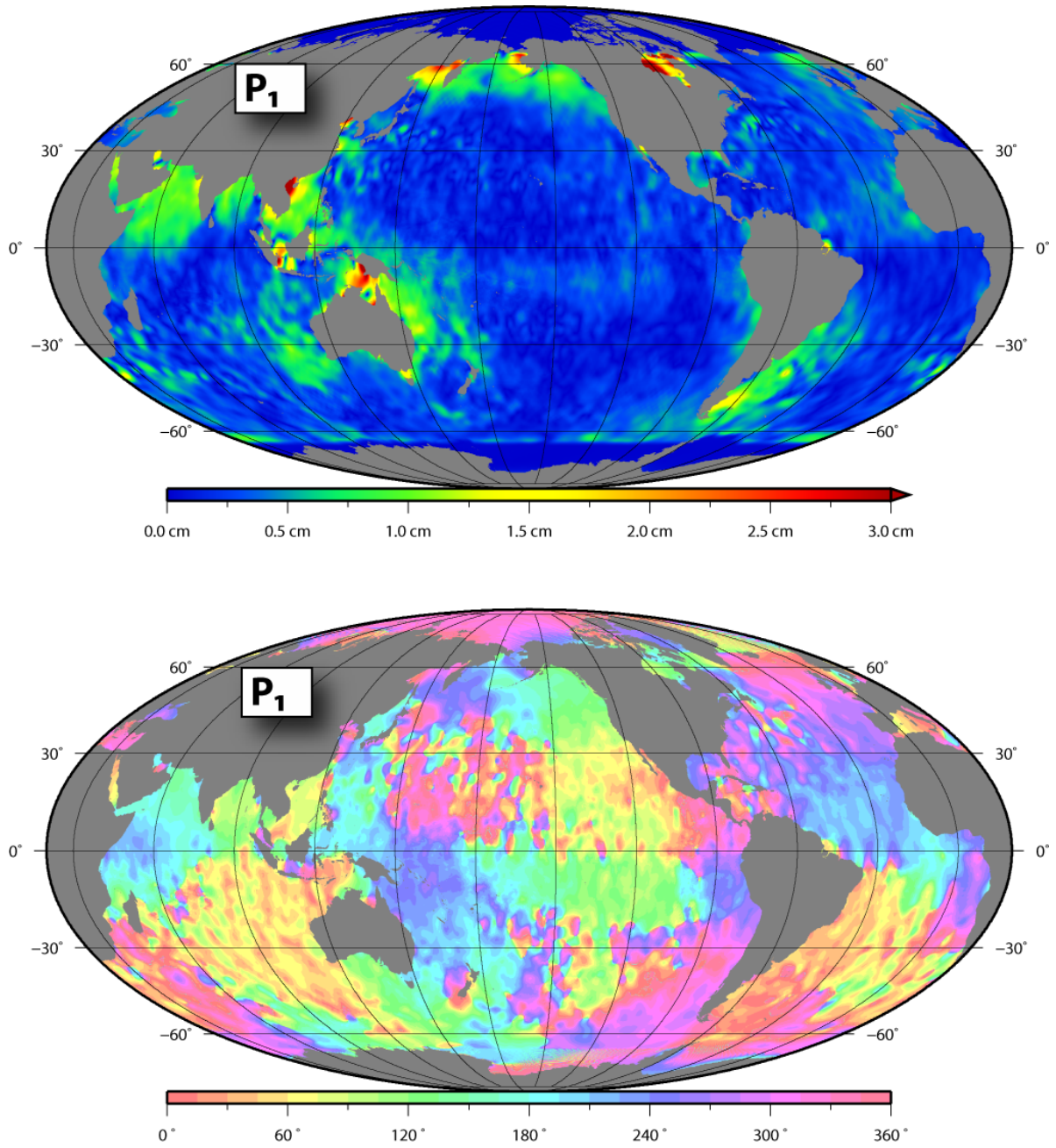


Figure A.8: Residual amplitude of P_1 tidal constituent w.r.t. FES2004

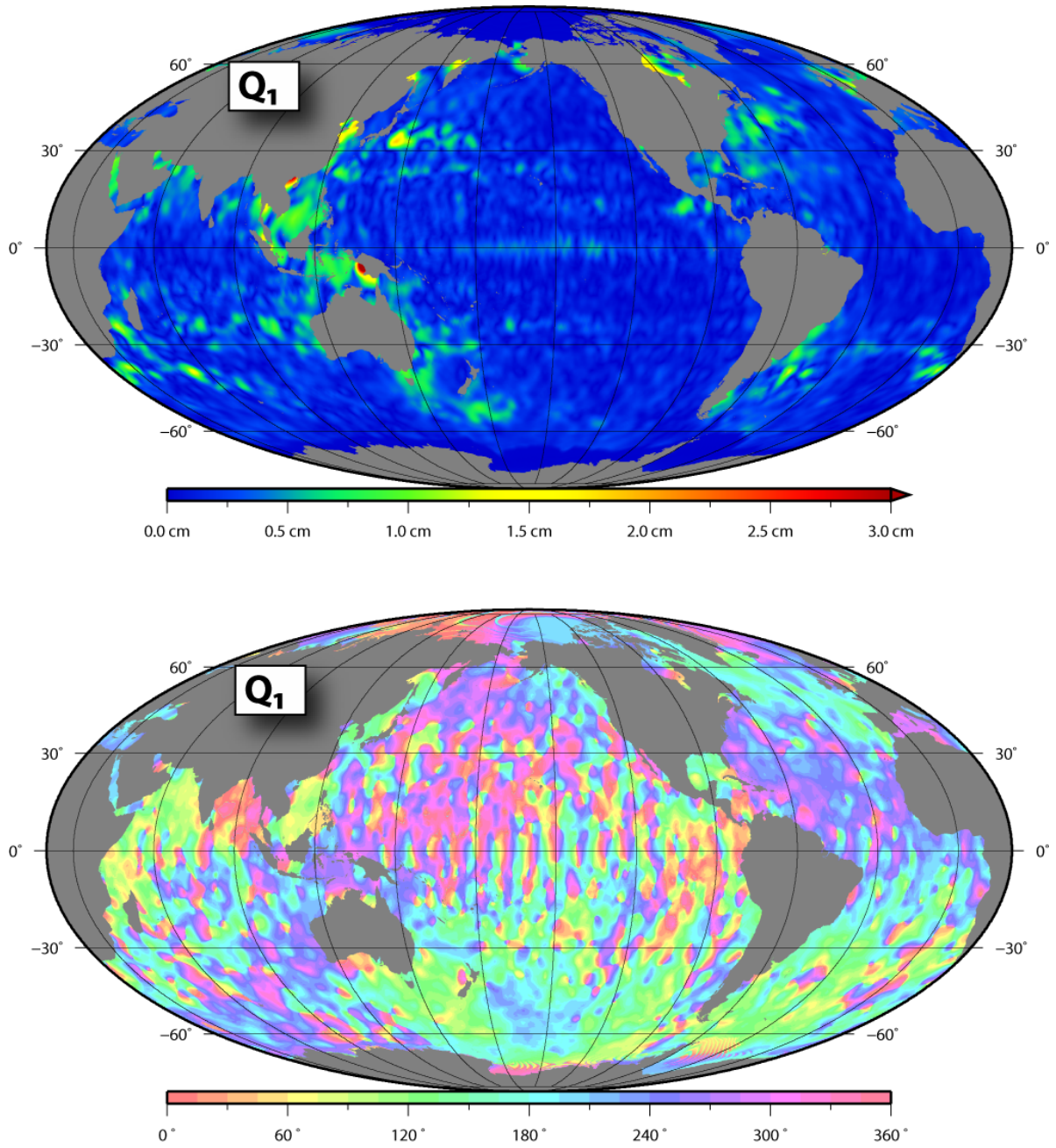


Figure A.9: Residual amplitude of Q_1 tidal constituent w.r.t. FES2004

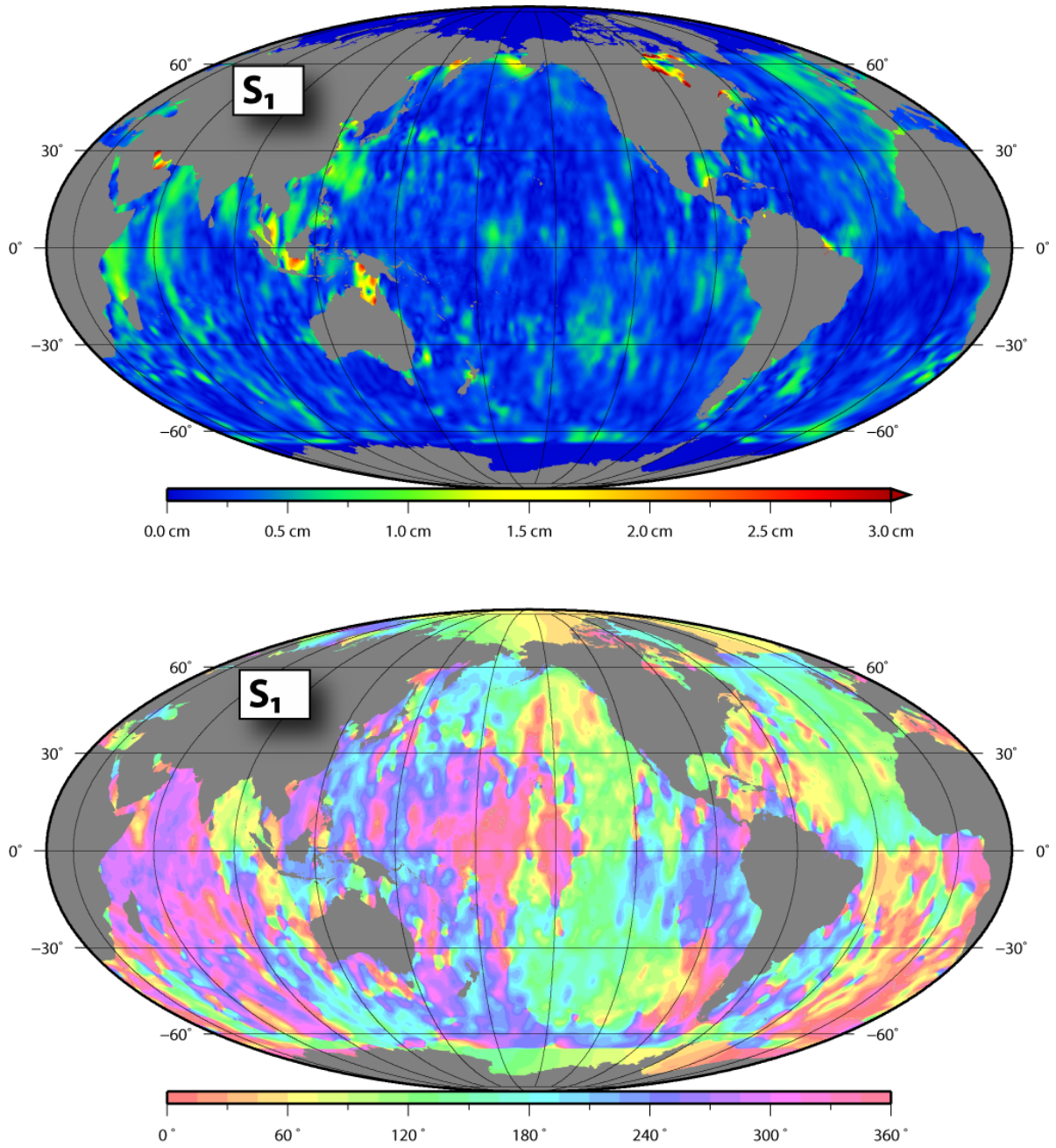


Figure A.10: Residual amplitude of S_1 tidal constituent w.r.t. FES2004

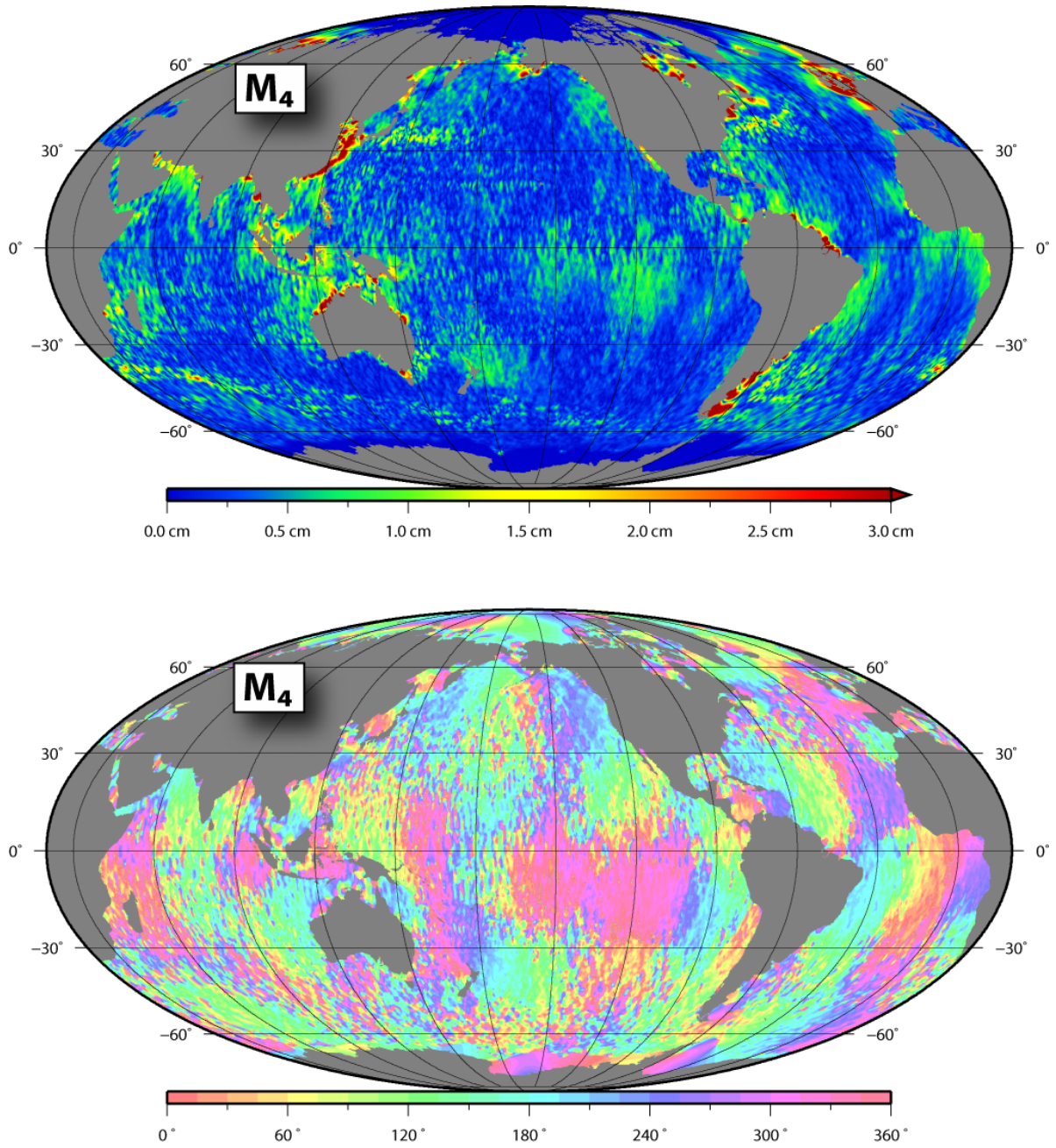


Figure A.11: Residual amplitude of M_4 tidal constituent w.r.t. FES2004

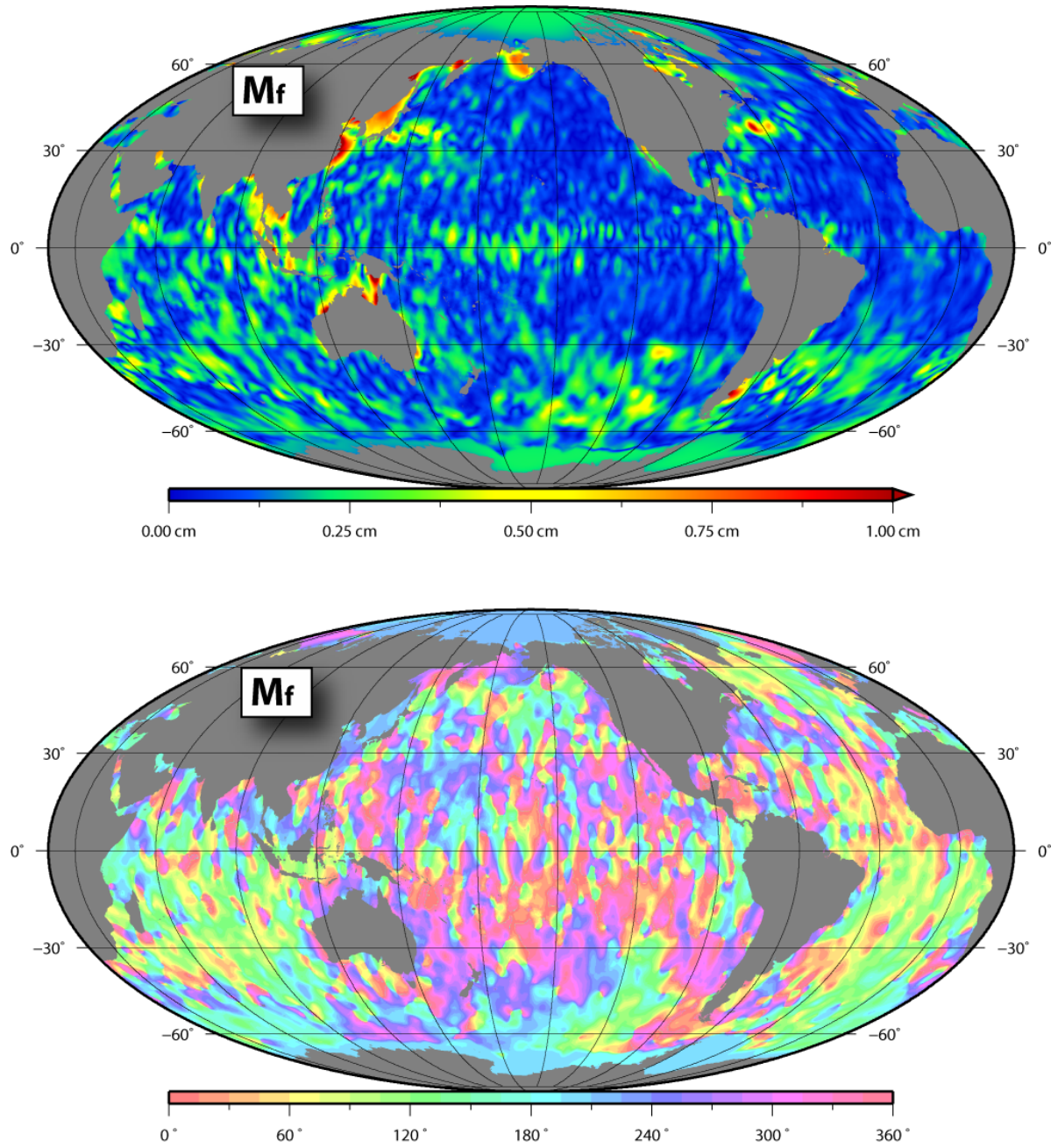


Figure A.12: Residual amplitude of M_f tidal constituent w.r.t. FES2004

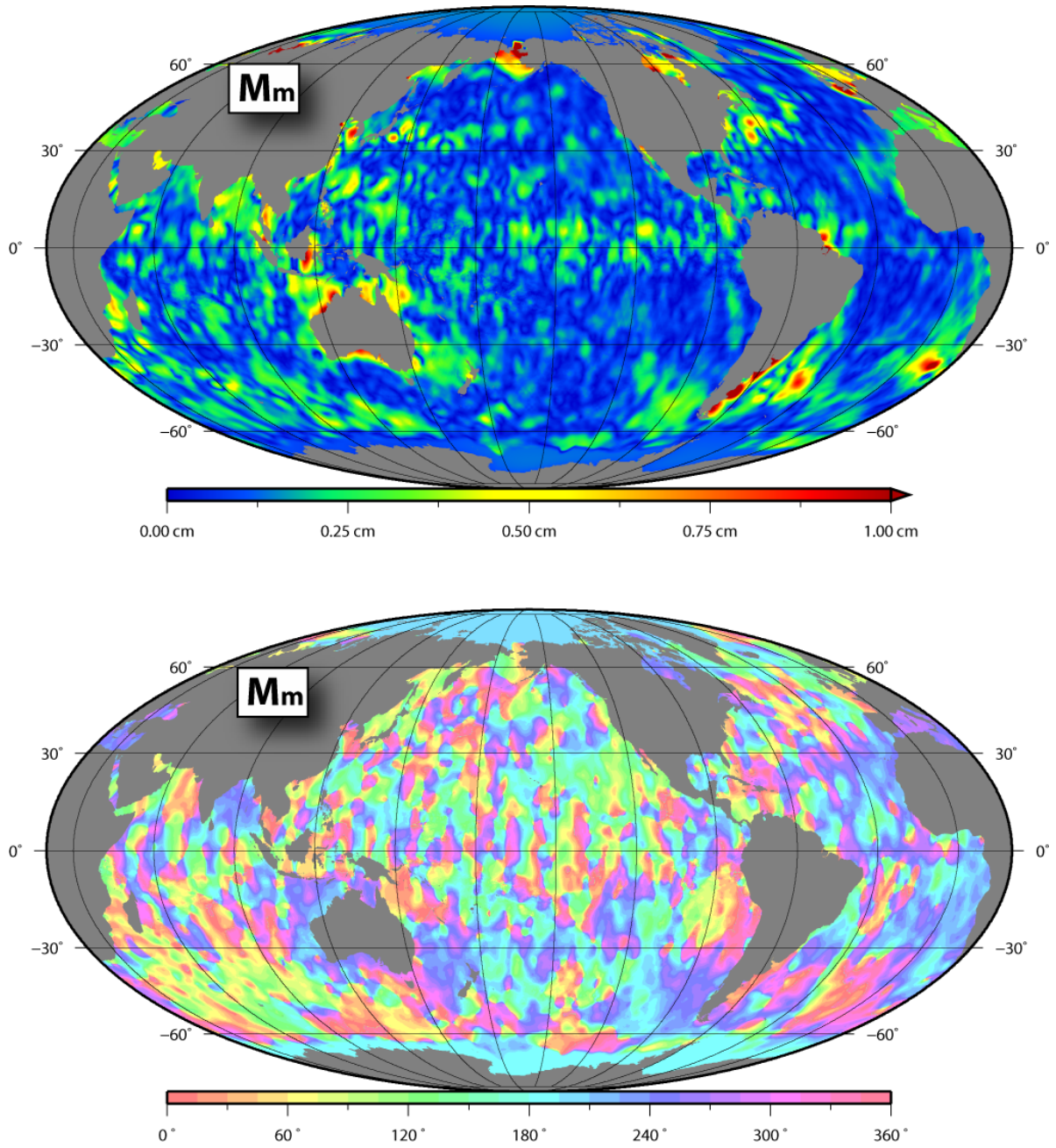


Figure A.13: Residual amplitude of M_m tidal constituent w.r.t. FES2004

A.6 Mission specific mean values

The a priori mean relative offsets (table 10) were already added to the mean values shown in the figures A.14, A.15, and A.16. The addition was necessary for the outlier elimination.

mission	offset [cm]
TOPEX/Poseidon	0
Jason-1	11.9
Jason-2	17.3
ERS-2	3.9
ENVISAT (GDR-A)	43.3
ENVISAT (GDR-B)	45.3

Table 10: A priori mean offsets added to the observations before tide analysis

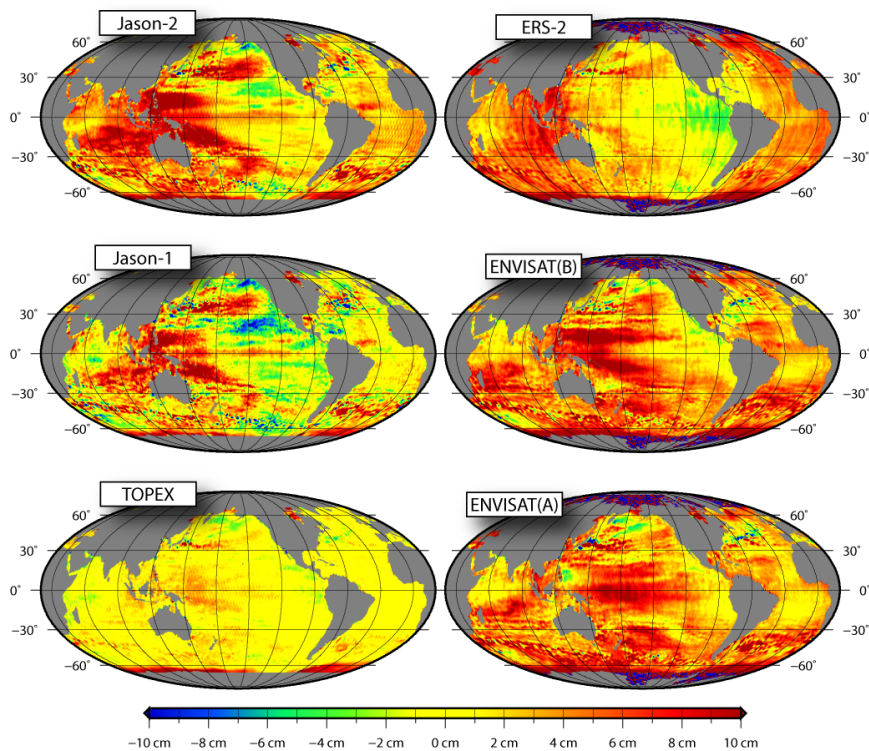


Figure A.14: Estimated mean values for the half weight width of 0.5°

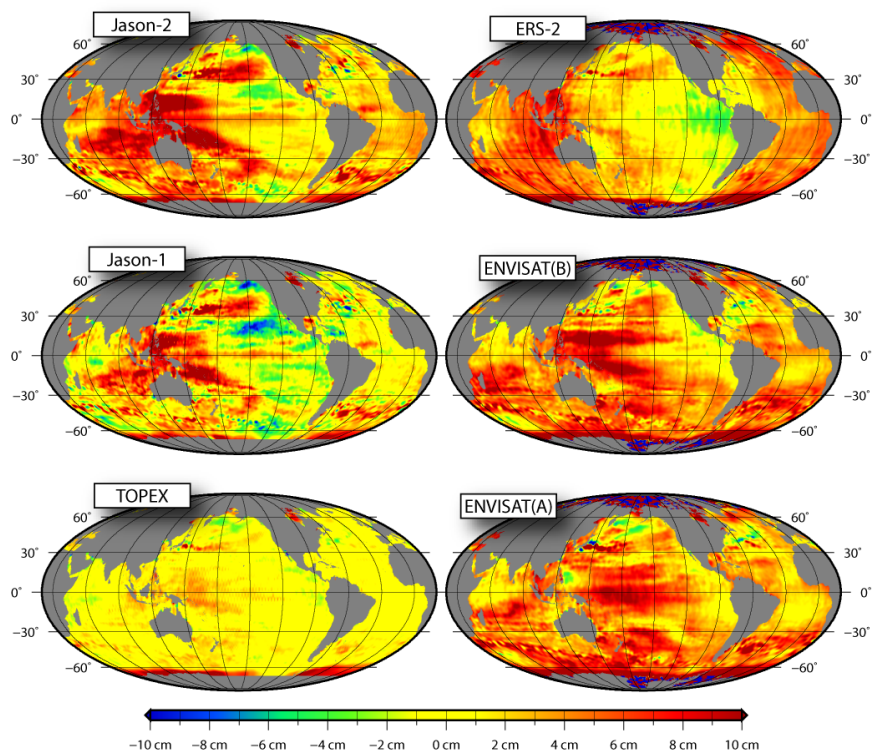


Figure A.15: Estimated mean values for the half weight width of 1.0°

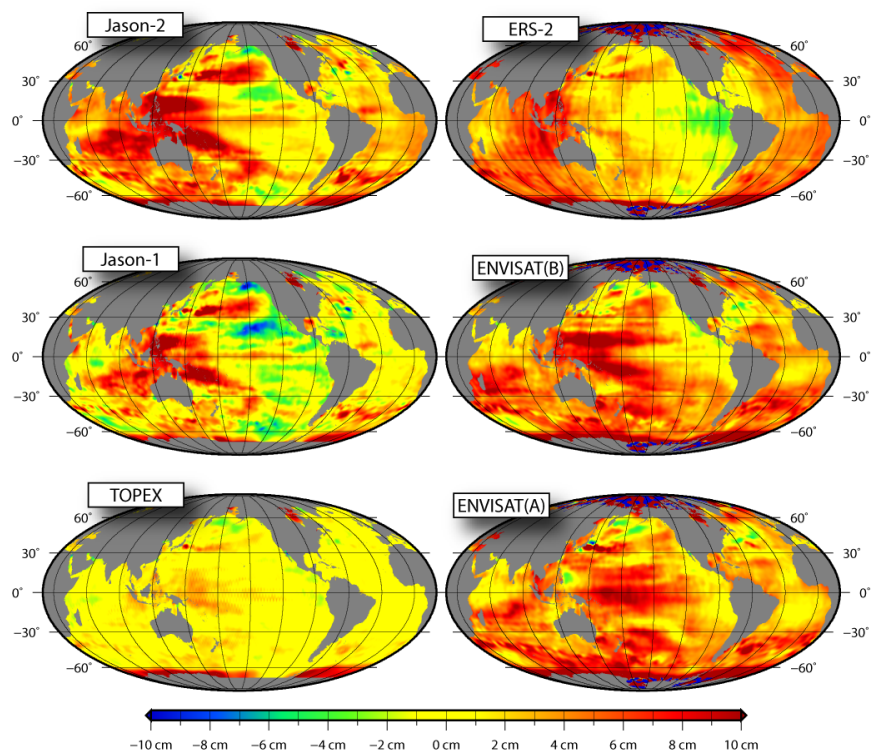


Figure A.16: Estimated mean values for the half weight width of 1.5°